Zoological Journal of the Linnean Society, 2022, **XX**, 1–37. With 12 figures.

Adaptation to graviportality in Rhinocerotoidea? An investigation through the long bone shape variation in their hindlimb

CHRISTOPHE MALLET[1,*], GUILLAUME BILLET[2], RAPHAËL CORNETTE[3] and ALEXANDRA HOUSSAYE[1]

[1]*Mécanismes adaptatifs et évolution (MECADEV), UMR 7179, MNHN, CNRS, 55 rue Buffon, CP 55, 75005 Paris, France*
[2]*Centre de Recherche en Paléontologie – Paris (CR2P), UMR 7207, MNHN, CNRS, SU, 8 rue Buffon, CP 38, 75005 Paris, France*
[3]*Institut de Systématique, Evolution, Biodiversité (ISYEB), UMR 7205, MNHN, CNRS, SU, EPHE, UA, 57 rue Cuvier, CP 50, 75005 Paris, France*

Received 22 July 2021; revised 20 December 2021; accepted for publication 12 January 2022

Weight support is a strong functional constraint modelling limb bones in heavy quadrupeds. However, the complex relations between bone shape, mass, size and body proportions have been poorly explored. Rhinocerotoidea is one of the groups showing the highest body mass reached by terrestrial mammals through time. Here, we explore the evolutionary variation of shape in hindlimb stylopod and zeugopod bones and its relationship with mass, size and gracility in this superfamily. Our results show that bones undergo a general increase in robustness towards high masses, associated with reinforcements of the main muscle insertions. The shape of the femur, carrying a marked phylogenetic signal, varies conjointly with mass, size and gracility, whereas that of the tibia appears related to gracility and mass only. The shape of the fibula does not vary according to that of the tibia. Moreover, congruent variation of shape between the distal part of the femur and the complete tibia underlines the potentially strong covariation of the elements constituting the knee joint. These results, coupled with those previously obtained from forelimb study, allow a better comprehension of the relationship between bone shape and mass among Rhinocerotoidea, and a refining of the concept of 'graviportality' in this superfamily.

ADDITIONAL KEYWORDS: appendicular skeleton – body mass – brachypody – functional morphology – geometric morphometrics – rhinoceros.

INTRODUCTION

Limb long bones, together with the muscles acting on them, fulfil essential functions like body support and locomotion in quadrupeds (Hildebrand, 1974). Consequently, their shape is regarded as strongly related to variations of body size, body mass and locomotor habits (Polly, 2007; Biewener & Patek, 2018). The convergent tendency of many quadruped lineages to reach high body mass across their evolution (Cope, 1887; Depéret, 1907; Raia *et al.*, 2012; Baker *et al.*, 2015; Bokma *et al.*, 2016) has led to repeated patterns of musculoskeletal constructions related to increase in size and mass. For more than a century, big animals have often been classified as 'graviportal', as opposed to 'cursorial' ones being characterized generally by smaller proportions (Hildebrand, 1974; Carrano, 1999). Skeletal features often associated with 'graviportality' in tetrapods are columnar and thick limbs, vertically oriented girdle bones, changes in limb segment proportions (reduction of the autopodium and lengthening of the stylopodium) and an increase in bone compactness (Gregory, 1912; Osborn, 1929; Hildebrand, 1974; Coombs, 1978; Eisenmann & Guérin, 1984; Biewener, 1989a, b; Bertram & Biewener, 1990; Houssaye *et al.*, 2016). Limitations in locomotor habits have also been observed in 'graviportal' animals,

*Corresponding author. E-mail: christophe.mallet@edu.mnhn.fr

like the inability to gallop in elephants or hippos (Alexander & Pond, 1992). The different combinations of all these modifications lead to a high diversity of body plans associated with a single given body mass (Hildebrand, 1974; Polly, 2007). However, while higher body mass is expected to influence modifications of the bone shape itself in 'graviportal' animals, the extent of those modifications is poorly studied among quadrupeds.

The superfamily Rhinocerotoidea, only represented by five surviving species today (Dinerstein, 2011), was extremely diverse during the Cenozoic. More than 100 species have been described in Eurasia, North America and Africa, with a notable diversity of ecological niches and locomotor morphologies (Prothero & Schoch, 1989; Cerdeño, 1998; Prothero, 2005; Biasatti *et al.*, 2018). Rhinocerotoidea displayed an important variation in body mass, ranging from less than 100 kg in *Hyrachyus* Leidy, 1871, the most ancient representative of the superfamily (Antoine, 2002; Bai *et al.*, 2017), to more than 10 tons in giant Paraceratheriidae (Fortelius & Kappelman, 1993; Prothero, 1998, 2013; Qiu & Wang, 2007) (Table 1). A convergent increase in body mass occurred in different lineages, in which many species frequently exceeded a body mass of 1 ton (Cerdeño, 1998). Throughout their evolutionary history, rhinocerotoids also underwent drastic modifications of their general body plan (e.g. limb morphologies suggesting a transition from 'cursorial' to 'graviportal'), their degree of brachypody (or gracility, i.e. reduction of their relative limb length), their ecological affinities (from open environments to presumed semi-aquatic lifestyles), their number of forelimb digits (tetradactyl or tridactyl manus), the presence of horns and the relative size of their head (Guérin, 1989; Prothero & Schoch, 1989; Prothero, 1998, 2005, 2013; Cerdeño, 1998; Antoine, 2002; Becker, 2003; Becker *et al.*, 2009; Bai *et al.*, 2017). Therefore, all these parameters may have covaried with the shape of their long bones.

Given the diversity in body mass, size and proportions encountered in this group over more than 50 Myr, this superfamily constitutes an excellent case study for the exploration of the evolution of long bone shape in relation to these morphological parameters. Only a few works previously explored the shape variation of the limb bones in modern or fossil rhinocerotoids, and in relation with mass, size or degree of brachypody/gracility (Guérin, 1980; Prothero & Sereno, 1982; Becker, 2003; Mallet *et al.*, 2019, 2020; Etienne *et al.*, 2020b). A recent integrative study explored this relationship between shape, size, mass and gracility on forelimb elements at the scale of the superfamily (Mallet *et al.*, 2021). Beyond a common general increase of bone robustness towards high body mass in Rhinocerotoidea, it also underlined that shape is not equally associated with size, mass and gracility among forelimb bones and that some groups (i.e. Paraceratheriidae, Teleoceratina) followed different allometric trends compared to the rest of the superfamily. The patterns of shape variation observed on the stylopodium reflect more the evolutionary history of the group than those observed on the zeugopodium history than that observed on the zeugopodium. Moreover, the study of some partial anatomical areas highlighted that proximal and distal epiphyses varied in relation to size, mass and gracility in different ways to the variation observed across the entire bone (Mallet *et al.*, 2021).

Building on these findings, our present study extends this approach to the hindlimb elements. Previous results on modern rhinos (Mallet *et al.*, 2019, 2020) indicated congruent shape variation between fore- and hindlimb stylopod elements (i.e. similar trends and high integration between the humerus and femur), with shape variation and covariation being likely more related to phylogeny than to body mass. Remarkable differences between fore- and hindlimb zeugopod elements were also highlighted, with a stronger correlation of shape variation with body mass in the forelimb. These differences between fore- and hindlimb elements may be related to divergent functional roles. Fore- and hindlimbs do not act similarly during quadrupedal mammal locomotion, the former function as brakes and are vital in directional change, the latter ensure body propulsion (Lessertisseur & Saban, 1967; Heglund *et al.*, 1982; Dutto *et al.*, 2006). Although all four limbs sustain the whole body mass, quadrupedal mammals bear a significantly higher part of their body mass on the forelimbs (Alexander, 1985; Henderson, 2006). This is particularly noticeable in rhinos, whose massive head, large muscle mass at the withers and presence of horns in some species, are likely to increase the proportion of the total body mass carried by the forelimbs (Henderson, 1999; Regnault *et al.*, 2013; Stilson *et al.*, 2016; Panagiotopoulou *et al.*, 2019). However, even if the length of the fore- and hindlimbs is relatively similar in most Rhinocerotoidea (Guérin, 1980), some taxa like Paraceratheriidae have a non-horizontal spine associated with having notably longer forelimbs than hindlimbs. This particular body plan likely changes which limbs support the largest part of the body mass and might also generate strong body mass-related shape variation on hindlimb elements, as has previously been observed on ankle bones of Perissodactyla (Etienne *et al.*, 2020b).

The exploration of shape variation in the hindlimb bones could help establish how body mass and its repartition across the animal is reflected in bone shape variation. Some similar trends as in the forelimb are likely to be observed, such as an increase of bone robustness towards high body mass (Mallet *et al.*, 2021). However, relationships between shape

Table 1. List of taxa, abbreviations, mean body masses and gracility indexes used in this study. Sources used to compile mean body mass and gracility index are given in the Supporting Information (Table S2)

Taxon	Abbreviation	Mean body mass (kg)	Gracility index (GI-MT3)
Acerorhinus zernowi	Ar. z.	700	0.26
Alicornops simorrense	Al. s.	875	0.29
Aphelops malacorhinus	Ap. ma.	889	0.25
Aphelops megalodus	Ap. me.	NA	0.26
Aphelops mutilus	Ap. mu.	1840	0.31
Brachypotherium brachypus	Br. b.	2327	0.35
Ceratotherium cf. *primaevum*	Ce. p.	NA	0.32
Ceratotherium neumayri	Ce. n.	1843	0.30
Ceratotherium simum	Ce. s.	2300	0.27
Chilotherium kowalevskii	Ch. k.	700	0.36
Coelodonta antiquitatis	Co. a.	2402	0.29
Coelodonta nihowanensis	Co. n.	NA	0.24
Diaceratherium aginense	Dia. ag.	1987	0.31
Diaceratherium asphaltense	Dia. as.	NA	0.31
Diaceratherium aurelianense	Dia. au.	1551	0.38
Diaceratherium lemanense	Dia. le.	1590	0.30
Diceratherium armatum	Dm. ar.	NA	0.21
Diceratherium tridactylum	Dm. t.	517	0.25
Dicerorhinus sumatrensis	Ds. su.	775	0.27
Diceros bicornis	Dc. b.	1050	0.27
Dihoplus megarhinus	Dh. m.	NA	0.27
Dihoplus pikermiensis	Dh. p.	1100	0.28
Dihoplus schleiermacheri	Dh. s.	2122	0.26
Elasmotherium sibiricum	E. s.	4500	0.24
Hoploaceratherium tetradactylum	Ho. t.	1197	0.26
Hyrachyus eximius	Hy. e.	67	0.17
Hyrachyus modestus	Hy. m.	NA	0.16
Hyracodon nebraskensis	Hn. n.	NA	0.16
Lartetotherium aff. *sansaniense*	Ds. sa.	NA	0.25
Lartetotherium sansaniense	L. s.	1204	0.24
Menoceras arikarense	Mc. a.	313	0.17
Metamynodon planifrons	Md. p.	1340	0.34
Nesorhinus philippinensis	N. p.	1086	0.28
Paraceratherium grangeri	Pa. g.	10 950	0.24
Peraceras hessei	Pe. h.	NA	0.26
Peraceras profectum	Pe. p.	NA	0.26
Plesiaceratherium mirallesi	Pl. m.	1268	0.25
Pleuroceros blanfordi	Pc. b.	1343	NA
Prosantorhinus douvillei	Ps. d.	NA	0.45
Protaceratherium minutum	Pt. m.	530	0.22
Rhinoceros sondaicus	R. s.	1350	0.35
Rhinoceros unicornis	R. u.	2000	0.27
Stephanorhinus jeanvireti	St. j.	NA	0.23
Stephanorhinus etruscus	St. e.	NA	0.24
Stephanorhinus hemitoechus	St. he.	1561	0.26
Subhyracodon mitis	Su. m.	NA	0.26
Subhyracodon occidentalis	Su. o.	NA	0.24
Teleoceras fossiger	Te. f.	1016	0.44
Teleoceras hicksi	Te. h.	1660	0.46
Teleoceras proterum	Te. p.	635	0.43
Trigonias osborni	Tg. o.	505	0.22
Trigonias wellsi	Tg. w.	NA	NA
Urtinotherium intermedium	U. i.	NA	0.23

variation and size, species mean body mass and degree of gracility might not be equivalent between the different hindlimb bones (femur, tibia and fibula). Moreover, the different roles of fore- and hindlimbs in weight support (forelimb) and propulsion (hindlimb) are predicted to be associated with notable differences in shape variation across the Rhinocerotoidea. Based on previous studies, we hypothesize: (1) strong congruences between shape variation and mass, and size and gracility in hindlimb bones; (2) differences between stylopodial and zeugopodial elements in their patterns of shape variation with respect to size, mass and gracility, but also (3) between complete and partial bones; (4) a link between phylogeny and bone shape to be reflected in different ways for the three studied bones [after the results of Mallet *et al.* (2019)]; and (5) differences in trends of shape variation between the fore- and the hindlimbs possibly related to their distinct functional roles.

MATERIAL AND METHODS

The studied sample was composed of 215 bones of modern and fossil species of Rhinocerotoidea housed in 14 institutions. The sample included 79 femora, 83 tibiae and 53 fibulae [see Supporting Information (Table S1) for the complete list of studied specimens] representing 53 taxa (five modern and 48 fossil species) belonging to almost all families of the superfamily Rhinocerotoidea (no representative of the recently-defined family Eggysodontidae could be included) (Fig. 1). Taxa were selected to include as much body shape and mass diversity as possible and to cover the largest temporal range, although this selection also depended greatly on material availability. Taxonomic attributions were verified or updated using recent literature, directly with specimen numbers when available, or using taxonomic lists and institution databases for each locality. We retained the most recent binomial names considered as correct following the International Commission on Zoological Nomenclature rules (see Supporting Information, Table S1).

We selected adult individuals with fully fused epiphyses and retained only complete bones displaying no or negligible taphonomic effects (e.g. shallow surface cracks not altering the global shape). We rejected specimens that were massively crushed or restored with plaster. Following the results of Mallet *et al.* (2021) indicating potentially different results between

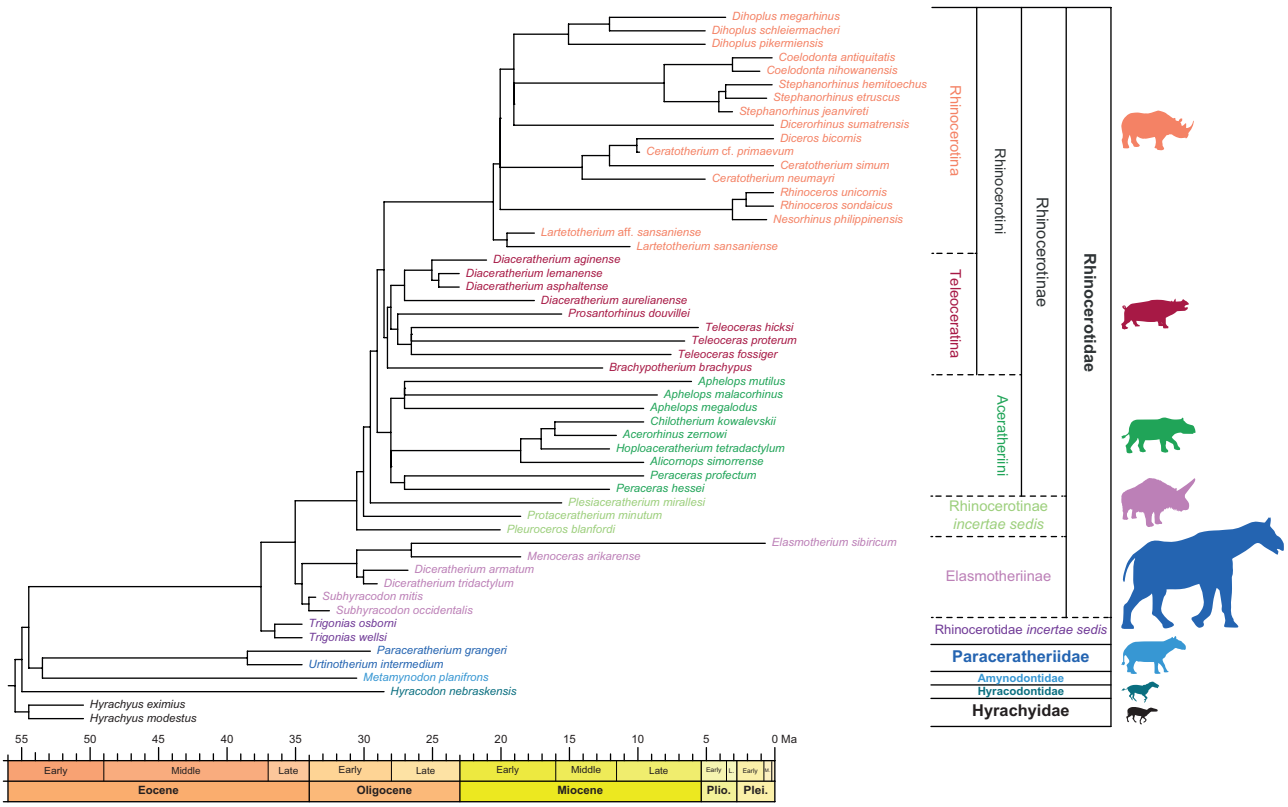

Figure 1. Composite cladogram of the studied species. Families, subfamilies, tribes and subtribes are defined by a colour code following the cladistic framework of Antoine *et al.* (2003) and Becker *et al.* (2013). All silhouettes representing a member of each group are at scale (provided by www.phylopic.org under the Creative Commons license).

complete and partial bones, we also considered incomplete bones in partial shape analyses (see below), as long as they were not crushed or distorted, in order to test if differences observed on forelimb bones may exist as well on hindlimb bones. Little information was available regarding sex for fossil specimens. Sexual dimorphism is known for some species and may slightly affect the shape of long bones (Guérin, 1980; Dinerstein, 1991; Mead, 2000; Zschokke & Baur, 2002; Mihlbachler, 2007; Chen *et al.*, 2010). However, following Mallet *et al.* (2019), we assumed that this intraspecific variation should be largely exceeded by interspecific shape changes. We selected up to three specimens per bone for each species. All anatomical terms (illustrated in Supporting Information, Fig. S1) follow classic veterinary terminology and anatomical works on Perissodactyla or only on rhinoceroses (Guérin, 1980; Federative Committee on Anatomical Terminology, 1998; Antoine, 2002; Prothero, 2005; Barone, 2010a; Heissig, 2012; Bai *et al.*, 2017). Locations of muscle insertions follow Etienne *et al.* (2021).

3D MODELS

Most of the bones were digitized using a structured-light 3D scanner (Artec Eva) with reconstructions using ARTEC STUDIO PROFESSIONAL [v.12.1.1.12 (Artec 3D, 2018)]. We also used this software to reconstruct bones broken in two or more pieces (without any missing parts) into a single complete mesh. Nine specimens were digitized with a photogrammetric approach, following Mallison & Wings (2014) and Fau *et al.* (2016). We used AGISOFT PHOTOSCAN [v.1.4.2 (Agisoft, 2018)] to reconstruct 3D models using sets of photos. Two specimens were digitized using medical computed tomography scanners at the Royal Veterinary College, London (Equine Hospital) and at the University of California, San Francisco (Department of Radiology & Biomedical Imaging). For these specimens, we extracted bone surfaces as meshes using AVIZO [v.9.5.0 (Thermo Fisher Scientific, 2018)]. As a few specimens lacked small parts, mostly on the shaft, we used GEOMAGIC STUDIO [v.2014.3.0.1781 (3D Systems Corporation, 2014)] to fill holes. We used the 'curvature filling' tool to ensure that the added polygons matched the curvature of the surrounding mesh. Finally, we decimated each mesh to reach 250 000 vertices and 500 000 faces using MESHLAB [v.2016.12 (Cignoni *et al.*, 2008)]. We performed our analyses on left bones, mirroring right bones when left ones were unavailable.

3D GEOMETRIC MORPHOMETRICS

We analysed the shape variation of our sample through a 3D geometric morphometrics approach, a methodology widely used to quantify and visualize the morphological differences between objects by comparing the spatial coordinates of points called landmarks (Adams *et al.*, 2004; Zelditch *et al.*, 2012). We quantified the bone shape by placing a set of anatomical landmarks and curve and surface sliding semi-landmarks on the meshes, following Gunz & Mitteroecker (2013) and Botton-Divet *et al.* (2016). We placed anatomical landmarks and curves on meshes using IDAV LANDMARK [v.3.0 (Wiley *et al.*, 2005)]. The geometric location of landmarks and sliding semi-landmarks is derived from previous morphometric works on rhinoceros long bones (Mallet *et al.*, 2019, 2020) to cover the shape diversity of the sample [see Supporting Information (Data S1) for details on landmark numbers and locations]. We created a template to automate the placement of surface sliding semi-landmarks for each bone. We chose a specimen [*Dicerorhinus sumatrensis* (Fischer, 1814) NHMUK ZE 1948.12.20.1] to be the initial specimen on which all anatomical landmarks, and curve and surface sliding semi-landmarks were placed. We selected this individual for its average shape and size ensuring that all points would be correctly projected on other bones despite the great shape and size ranges of the sample. This specimen was then used as template for the projection of surface sliding semi-landmarks on the surface of all other specimens. Projection was followed by a relaxation step to ensure that projected points matched the actual surface of the meshes. We then slid curve and surface sliding semi-landmarks to minimize the bending energy of a thin plate spline (TPS) between each specimen and the template at first, and then four times between the result of the previous step and the Procrustes consensus of the complete data set. Therefore, all landmarks could be treated at the end as geometrically homologous (Gunz *et al.*, 2005; Gunz & Mitteroecker, 2013).

Since we chose to work at the species level, we computed and analysed species mean shapes (Botton-Divet *et al.*, 2017; Serio *et al.*, 2020). After the sliding step, we computed a first Generalized Procrustes Analysis (GPA) with all specimens to remove the effect of size, location and orientation of the different landmark conformations (Gower, 1975; Rohlf & Slice, 1990). Then we computed the Procrustes consensus (or mean shape) of each species in the same geometric space. We superimposed these Procrustes consensuses in a second GPA in order to pool all species means in a single morphospace. We repeated this process for each bone separately. Because our data set contained more variables than observations, we computed a Principal Component Analysis (PCA) to reduce dimensionality (Baylac & Frieß, 2005; Gunz & Mitteroecker, 2013) and visualize the distribution of the species in the morphospace. We also computed theoretical shapes associated with both the minimum and the maximum

of the first two components of PCAs using a TPS deformation of the mean shape of our sample in each case. Theoretical shapes have also been used to produce colour maps of the location and intensity of the shape deformation between maximal and minimal values of regression: for each bone, the shape associated with the minimum values was coloured depending on its distance to the shape associated with the maximum values. We then plotted phylogenetic relationships between taxa (see below) in the morphospace. In order to visualize the whole shape variation, we computed Neighbour Joining (NJ) trees on all PC scores and compared these to the results of the PCAs on the two first PC scores. We performed projection, relaxation, sliding processes, GPAs, PCAs and theoretical shape computation using the 'Morpho' package [v.2.8 (Schlager, 2017)] in the R environment [v.3.5.3 (R Core Team, 2014)]. We plotted phylogeny on the morphospace using the 'geomorph' package [v.3.2.1 (Adams & Otárola-Castillo, 2013)]. We computed NJ trees using the 'ape' package [v.5.3 (Paradis & Schliep, 2019)].

Analyses on partial bones

Our observations on fossil long bones of rhinoceros showed that redundant breakage patterns were observable due to various taphonomic agents throughout diagenesis [e.g. high sedimentary pressure on weak anatomical areas, scavenger action on marrow-rich parts—see Guérin (1980); Hullot & Antoine (2020)]. As on the forelimb, some parts of the hindlimb bones were often damaged or absent in fossil specimens (Mallet *et al.*, 2021). This was notably the case on the femur, where the femoral head, the third trochanter, the medial lip of the trochlea and the condyles were frequently too damaged to be included in shape analyses.

To overcome these taphonomic problems and include as many relevant specimens as possible (i.e. cover the broadest range of body mass and size as possible), we performed analyses on isolated proximal and distal parts of the femur, using the same protocol as described in Mallet *et al.* (2021). Following Bardua *et al.* (2019), we used curve and sliding semi-landmarks to define artificial lines acting as a limit for the sliding of surface semi-landmarks and to virtually remove damaged or missing parts from analyses. These limit lines involved at least one anatomical landmark to ensure that they were geometrically homologous on all specimens. We also placed them on complete bones, which were all included in the analyses on partial bones. We finally removed limit lines after the sliding process and before the GPA to consider only true biological shape information in our analyses. We used two data sets on partial bones, for the proximal and distal halves of the femur, respectively [see Supporting Information (Data S1) for details on landmarks and sliding semi-landmarks in templates of partial bones].

Phylogenetic framework

Recent publications refined phylogenetic relationships in Rhinocerotoidea (Wang *et al.*, 2016; Tissier *et al.*, 2018, 2020; Bai *et al.*, 2020) and in Ceratomorpha (Bai *et al.*, 2020), although not including all genera of rhinocerotoids currently known worldwide. Therefore, no comprehensive and consensual phylogeny of the whole superfamily Rhinocerotoidea exists to date. To take into account the effect of phylogeny on shape variation, we constructed a composite cladogram using trees previously computed on craniodental and postcranial characters or molecular data. Using Mesquite (Maddison & Maddison, 2021), we reconstructed interspecific relationships, branch lengths and occurrence dates after the works of Cerdeño (1995), Antoine (2002), Antoine *et al.* (2003, 2010), Prothero (2005), Boada-Saña (2008), Piras *et al.* (2010), Becker *et al.* (2013), Lu (2013), Wang *et al.* (2016), Averianov *et al.* (2017), Tissier *et al.* (2018, 2020), Bai *et al.* (2020). We used the cladistic framework of Antoine *et al.* (2003) and Becker *et al.* (2013) to define families, subfamilies, tribes and subtribes (Fig. 1). To date, the relationships between the five modern taxa remain controversial, especially regarding the position of the Sumatran rhinoceros (*Dicerorhinus sumatrensis*) and its extinct relatives (e.g. Tougard *et al.*, 2001; Orlando *et al.*, 2003; Fernando *et al.*, 2006; Price & Bininda-Emonds, 2009; Steiner & Ryder, 2011; Yuan *et al.*, 2014; Welker *et al.*, 2017; Cappellini *et al.*, 2019; Antoine *et al.*, 2021). These uncertainties are likely due to a hard polytomy at the base of the crown group containing the five modern species (Willerslev *et al.*, 2009; Gaudry, 2017). Although recent genomic analyses tend to indicate that African and Asiatic rhinos constitute two sister groups (Liu *et al.*, 2021), we considered a hard polytomy in our analyses and we addressed phylogenetic uncertainties using a Nearest Neighbour Interchange (NNI) procedure (see below).

To address the effect of phylogenetic relationships on shape data for each bone, we evaluated their phylogenetic signal by computing a multivariate K statistic (K_{mult}) on PC scores (Adams, 2014). This index compares the rate of observed morphological change with that expected under a Brownian Motion model on a given phylogeny (Blomberg *et al.*, 2003; Adams, 2014). As the K_{mult} computation requires fully bifurcating trees, we removed polytomies using the function *multi2di* in the 'ape' package (Paradis & Schliep, 2019). This function resolves polytomies by randomly creating a new branch with a null length from one branch of the polytomous node (Swenson, 2014; Paradis & Schliep, 2019). We then computed K_{mult}

values using the function *K.mult* in the 'phylocurve' package (Goolsby, 2015).

Body mass, centroid size and gracility index

As in Mallet *et al.* (2021) for the forelimb, we addressed the relation of three variables related to body proportions and size—body mass, centroid size of the bone and gracility index—with the shape of each long bone of the hindlimb within Rhinocerotoidea. We retrieved mean body mass (BM) of each species from the literature, compiling up to three estimations per species to compute mean BMs (see Table 1; Supporting Information, Table S2). However, BM estimations can be highly heterogeneous for a single species depending on the considered method and morphological proxy (mostly on dental and cranial measurements and less frequently on postcranial ones), the specimen developmental stage or the geological formation. Moreover, equations for BM estimation were rarely developed taking into account Perissodactyla or rhinoceroses, resulting in potentially biased results for fossil Rhinocerotoidea (Prothero & Sereno, 1982). We managed to collect BM estimation for only 34 of the 53 taxa constituting our sample. Consequently, we also consider the centroid size (CS) of each bone, which is classically used to address allometric variation, i.e. the shape variation linked to size (Zelditch *et al.*, 2012; Mitteroecker *et al.*, 2013; Klingenberg, 2016; Hallgrímsson *et al.*, 2019). CS is defined as the square root of the sum of the square of the distance of each point to the centroid of the landmark set (Zelditch *et al.*, 2012). CS is known to be a good proxy of the mass of an animal (Ercoli & Prevosti, 2011; Cassini *et al.*, 2012), notably for limb bones of rhinoceros (Mallet *et al.*, 2019; Etienne *et al.*, 2020b). In addition, given the large range of body shapes within Rhinocerotoidea (Fig. 1) and the fact that the same mass can be associated with both a slender or a robust body condition, we used the mean gracility index computed on the third metatarsal (GI-MT3) as an estimator of the degree of brachypody of the hindlimb (see Table 1; Supporting Information, Table S2). This index is computed by dividing the transverse width of the third metatarsal by its maximal length and has been used widely in rhinocerotoid studies, together with the same index computed on the third metacarpal for the forelimb (Colbert, 1938; Arambourg, 1959; Guérin, 1980; Cerdeño, 1998; Becker, 2003; Becker *et al.*, 2009; Scherler *et al.*, 2013). Among Rhinocerotoidea, the higher the GI-MT3 value, the shorter the pes length: species with a high GI-MT3 value are considered as more brachypodial (or less gracile) than species with a low value. We computed this index by measuring third metatarsals when available in collections or compiling up to three GI-MT3 values from the literature to compute mean GI-MT3. These metatarsals were mostly associated with long bones for modern species and mostly associated with a similar locality for fossil species (Supporting Information, Table S2). We addressed the effect of phylogeny on log-transformed CS, log-transformed cubic root of the mean BM and log-transformed mean GI-MT3 using the univariate K statistic (Blomberg *et al.*, 2003). We tested for correlation between these three variables respectively using a linear regression on Phylogenetic Independent Contrasts (Felsenstein, 1985). We used the function *contMap* of the 'phytools' package (Revell, 2012) to plot these three variables along the phylogeny.

Variation patterns, notably covariation, can be analysed at different levels: across species (evolutionary variation), within a species at a single developmental stage (static variation), or within a species across developmental stages (ontogenetic variation) (Klingenberg, 2014). Here, we investigated the evolutionary covariation of bone shape with each of the three variables (BM, CS, GI-MT3) considering a multivariate approach using Phylogenetic Generalized Least Squares (PGLS), a regression model taking into account the phylogenetic framework and computed here on Procrustes coordinates to quantify the shape variation related to CS, BM and GI-MT3 (Martins & Hansen, 1997; Rohlf, 2001; Klingenberg & Marugán-Lobón, 2013; Adams & Collyer, 2018). We used the function *procD.pgls* (with 1000 iterations) of the 'geomorph' package [v.3.2.1 (Adams & Otárola-Castillo, 2013)], suited for 3D geometric morphometric data. As the function *procD.pgls* uses a Brownian Motion model of evolution to compute PGLS, which assumes non-directional trait changes, other models might assume a different computational hypothesis. To account for these changes depending on the considered model, we also computed PGLS under a Phylogenetic Ridge Regression model of evolution (Castiglione *et al.*, 2018). Phylogenetic Ridge Regression takes into account variations of evolutionary rates along the different branches of a phylogenetic tree, and potential accelerations and decelerations of the phenotypic changes among groups in a more accurate way than a Brownian Motion model. Therefore, we used the function *PGLS_fossil* of the 'RRphylo' package [v.2.5.0 (Castiglione *et al.*, 2018)] to compute PGLS with a Phylogenetic Ridge Regression model and compared it to the results obtained under a Brownian Motion model in order to see whether our results were robust to model variations.

As previously mentioned, the phylogeny of Rhinocerotoidea remains debated for both extant and extinct taxa and is frequently renewed by the determination of new representatives (Tissier *et al.*, 2020; Bai *et al.*, 2020). Consequently, we assessed the effect of potential uncertainty in taxa position in the

phylogeny on PGLS by using an NNI procedure. The NNI algorithm generates new trees by swapping two adjacent branches of a specified tree (Felsenstein, 2004). We generated new trees using the *nni* function of the package 'phangorn' (Schliep, 2011) and computed PGLS with these rearranged trees to estimate the ranges of R^2 and *P* values. It should be noted that the R^2 value of a PGLS should not be considered comparable with that of an ordinary least squares regression (Ives, 2019; Billet & Bardin, 2021). Consequently, our interpretations of data will rely as little as possible on these R^2 values alone.

We considered all statistical tests as significant for *P*-values ≤ 0.01. However, given that recent works call for a continuous approach of the *P*-value (Ho *et al.*, 2019; Wasserstein *et al.*, 2019), we chose to mention results having a *P*-value up to 0.05 as well.

RESULTS

Correlation between BM and GI-MT3

Both mean BM and mean GI-MT3 carry a significant phylogenetic signal (K_{BM} = 1.75, $P < 0.01$; $K_{GI\text{-}MT3}$ = 1.08, $P < 0.01$), but are only marginally correlated to each other when taking into account phylogenetic relationships ($P = 0.06$). The evolution of both parameters along the phylogeny (Fig. 2) highlights that the evolution of these parameters within the superfamily is decoupled in some taxa

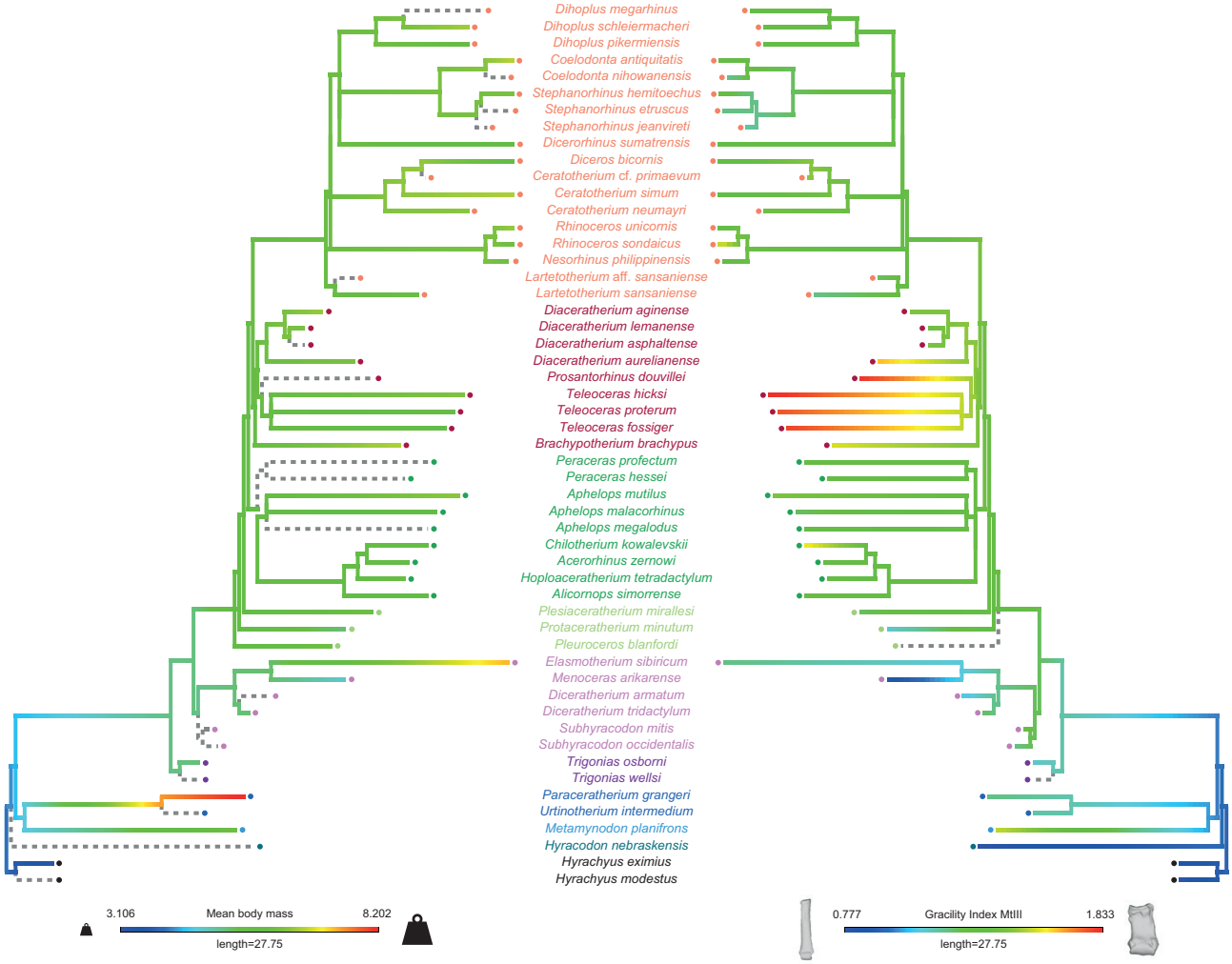

Figure 2. Evolution of BM and GI-MT3 along the phylogeny for the studied species. Left: mean BM. Right: mean GI-MT3. Computations were made on the log-transformed cubic root of mean BM and the log-transformed GI-MT3. Values at nodes and along branches were reconstructed based on a Brownian Motion model of evolution (Revell, 2012). Colour codes for taxa follow Figure 1. Evolution of the third metatarsal shape depending on the GI-MT3 value is illustrated by specimens *Hyrachyus eximius* AMNH FM 12675 (minimum) and *Teleoceras fossiger* YPM VP 039358 (maximum).

like Paraceratheriidae, Teleoceratina and, to a lesser extent, large Elasmotheriinae.

Differences in PGLS between Brownian Motion and phylogenetic ridge regression

Similar results are obtained between PGLS computed under a Brownian Motion model (using the geomorph functions) and under a Phylogenetic Ridge Regression (RR) model (using the RRphylo functions) [see Supporting Information (Table S3) for a detailed comparison between models]. Significant regressions under a Brownian Motion model remain significant under an RR model, in addition non-significant results under a Brownian Motion model remain non-significant under an RR model. We note low variations of R^2, *P*-values and shape deformations between the two models. Only regression plots show marked differences, with a much higher spread of specimens in those obtained under an RR model, making their interpretation more difficult. For these reasons, we will present only results obtained under a Brownian Motion model in the following sections.

Femur—complete bone

Shape data for the complete femur carry a strong phylogenetic signal ($K_{mult} = 0.93$, $P < 0.01$). The distribution of the species both in the NJ tree (Fig. 3A) and in the phylomorphospace (Fig. 4) is strongly reminiscent of the phylogenetic relationships between taxa. Along the NJ tree, Hyrachyidae group with Hyracodontidae, Elasmotheriinae (all of small size in the absence of *Elasmotherium* Fischer, 1808) and some Rhinocerotinae [*Protaceratherium* Abel, 1910 and *Peraceras* (*Pe.*) *profectum* (Matthew, 1899)]. *Paraceratherium* Forster-Cooper, 1911 groups with two species of *Aphelops* Cope, 1874, while *Metamynodon* Scott & Osborn, 1887 is close to some Aceratheriini (*Hoploaceratherium* Ginsburg & Heissig, 1989) as well as some Rhinocerotina (*Lartetotherium* Ginsburg, 1974). Although Aceratheriini are dispersed along the tree, most of the Rhinocerotina are grouped together. Similarly, Teleoceratina form a homogeneous cluster despite the presence of *Peraceras* (*Pe.*) *hessei* Prothero & Manning, 1987. Conversely, *Chilotherium* Ringström, 1924 and *Pleuroceros* Roger, 1898, two highly brachypodial taxa, plot within Rhinocerotina, far from other brachypodial species like *Teleoceras* Hatcher, 1894. On the phylomorphospace, the first two axes gather 58.4% of the global variance. PC1, which carries 42.9% of the variance, displays a structure similar to the general organization of the NJ tree. Small taxa such as *Hyrachyus* and *Hyracodon* Leidy, 1856 plot toward positive values. Towards moderately negative values, small Elasmotheriinae plot near *Metamynodon*, *Trigonias* Lucas, 1900 and small Aceratheriini. The giant paraceratheriid *Urtinotherium* Chow & Chiu, 1963 plots near small taxa like *Trigonias* or *Protaceratherium*, but also near *Metamynodon*. Towards the most negative values, large Aceratheriini are mixed with Teleoceratina and Rhinocerotina. Along PC2, which carries 15.5% of the variance, Rhinocerotina form a homogeneous cluster plotting towards negative values, together with *Metamynodon*, *Hyrachyus* and *Subhyracodon* Brandt, 1878. Teleoceratina and Aceratheriini (except *Aphelops* (*Ap.*) *malacorhinus* Cope, 1878) group together with *Urtinotherium*, *Subhyracodon mitis* (Cope, 1875) and *Hyracodon* towards positive values.

The shape variation along PC1 is mainly related to the bone robustness (Fig. 4; Supporting Information, Fig. S2A). Less negative values are associated with a slender bone showing a rounded hemispherical head with a narrow neck; a proximally developed greater trochanter tuberosity protruding over the head; an oval fovea capitis; a third trochanter situated at the first proximal third of the shaft, more developed caudally than laterally; a craniocaudally straight shaft; a relatively symmetrical distal trochlea with a poorly developed medial lip; a long and narrow trochlear groove running caudally to the shaft; a distal epiphysis showing medial torsion relative to the shaft; and relatively symmetrical medial and lateral condyles. Conversely, negative values are associated with a thick and massive bone, with a general hourglass shape in cranial view; a more flattened and wide head with a large neck; a greater trochanter tuberosity poorly developed proximally and not protruding over the head; a small rounded fovea capitis; a strong third trochanter clearly protruding laterally and cranially from the shaft; a shaft slightly curved in the caudal direction; a strongly asymmetrical trochlea with a broad medial lip; a short and wide trochlear groove; a distal epiphysis oriented cranially relative to the shaft; and a medial condyle more developed than the lateral one. Along PC2, the shape variation mostly concerns the development of the trochanters and the relative proportions of the epiphyses. The theoretical shape associated with negative values shows proximal and distal epiphyses of similar mediolateral width; a lesser trochanter situated just below the head and above the third trochanter on the opposite side; and a third trochanter developed in both cranial and lateral directions. Conversely, the shape associated with positive values displays a head and a relatively larger head and greater trochanter; a head oriented more proximally; lesser and third trochanters facing each other on the medial and lateral side of the shaft, respectively; a third trochanter reduced to a bony ridge; and a medial lip of the trochlea more developed cranially.

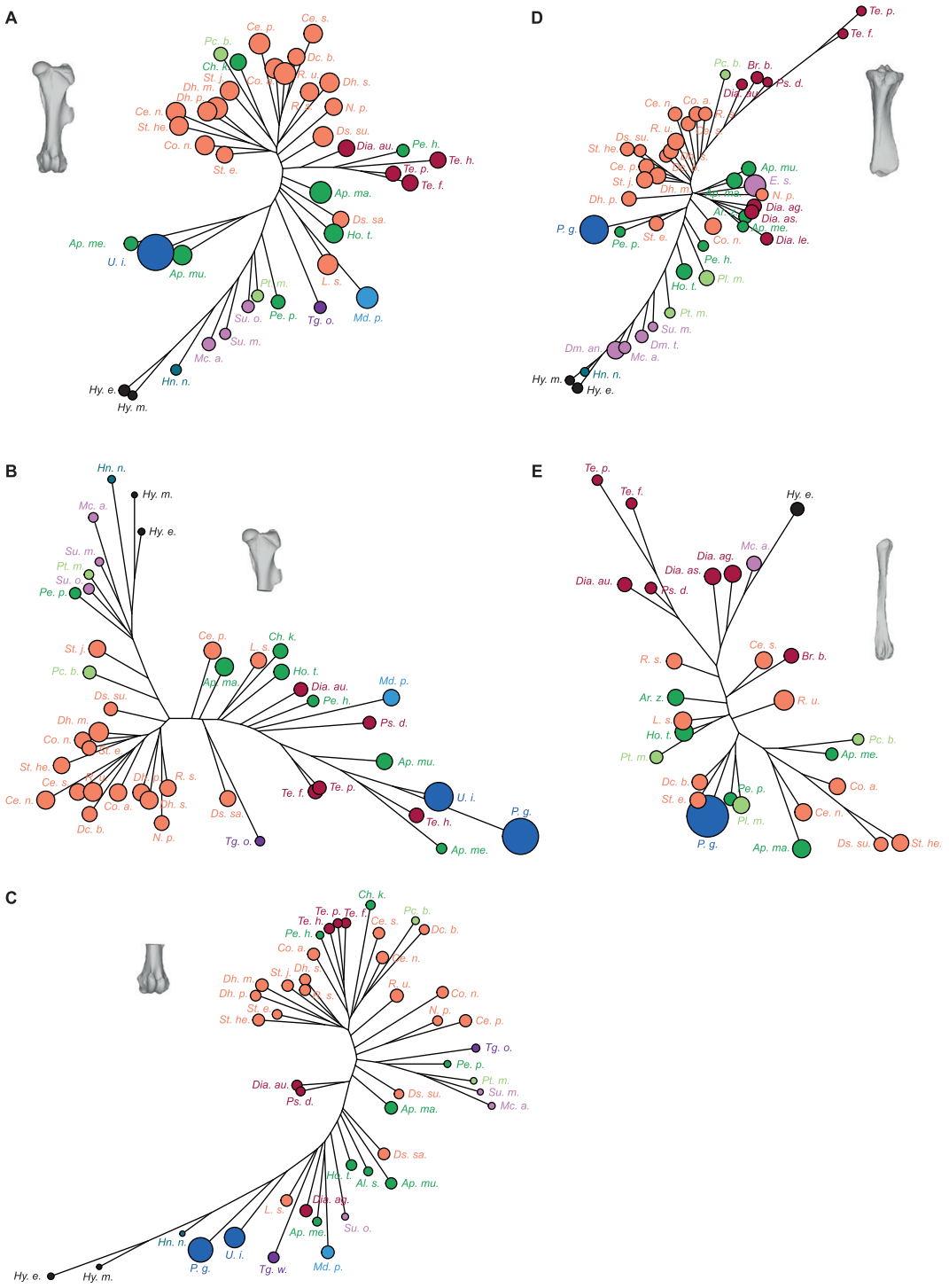

Figure 3. Neighbour Joining trees computed on all PC scores obtained from the PCAs performed on shape data. Colour codes follow Figure 1 and abbreviations follow Table 1. Point size is proportional to the mean log centroid size of each species. A, complete femur; B, proximal partial femur; C, distal partial femur; D, tibia; E, fibula.

The centroid size of the complete femur bears a significant phylogenetic signal (K_{CS} = 1.05, P < 0.01) and is significantly correlated with BM (r = 0.70, P < 0.01), but not with GI-MT3 (P = 0.37) (Table 2). PGLS results indicate that shape is significantly correlated with CS, BM and GI-MT3. PGLS computed on NNI trees highlight that variations in phylogenetic relationships may result in marginally non-significant

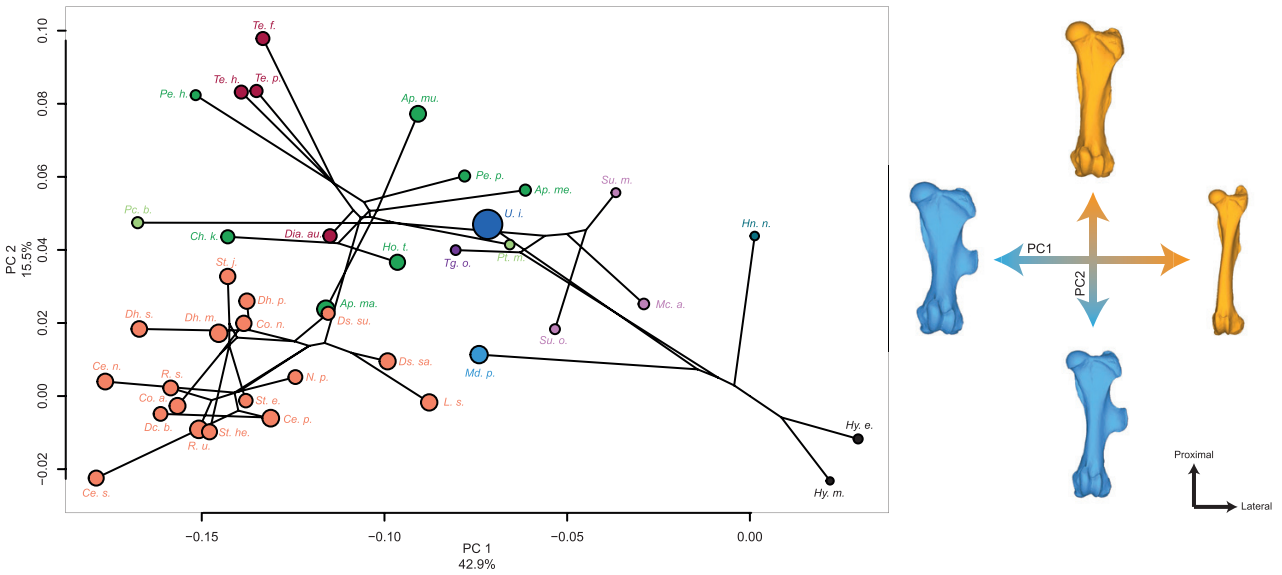

Figure 4. Results of the PCA performed on morphometric data of the complete femur and shape variation associated with the first axis of the PCA (cranial view). Blue: negative side of the axis. Orange: positive side of the axis. Phylogenetic relationships are plotted in the morphospace. Colour codes follow Figure 1 and abbreviations follow Table 1. Point size is proportional to the mean log centroid size of each species.

Table 2. Results of the Pearson's correlation tests between centroid size (CS), and mean body mass (BM) and mean gracility index (GI-MT3), respectively, for each bone (computed on Phylogenetic Independent Contrasts). r: Pearson's correlation coefficient value; *t*: student distribution value; d.f.: degrees of freedom; *P*: *P*-value. Significant results (for $P < 0.01$) are indicated in bold

Bone	Variables	r	*t*	d.f.	*P*
Femur (complete)	**CS ~ BM**	**0.70**	**4.72**	**23**	**< 0.01**
	CS ~ GI	0.15	0.91	36	0.37
Femur (proximal partial)	**CS ~ BM**	**0.91**	**10.44**	**24**	**< 0.01**
	CS ~ GI	0.22	1.36	38	0.18
Femur (distal partial)	**CS ~ BM**	**0.86**	**8.46**	**26**	**< 0.01**
	CS ~ GI	0.16	0.99	40	0.32
Tibia	**CS ~ BM**	**0.72**	**5.23**	**26**	**< 0.01**
	CS ~ GI	-0.23	-1.51	39	0.14
Fibula	**CS ~ BM**	**0.71**	**4.46**	**20**	**< 0.01**
	CS ~ GI	-0.28	-1.41	24	0.17

correlations for CS and GI-MT3 but mean *P*-values are strongly significant (Table 3). In the regression plot of shape against CS, the distribution of taxa shows a relatively poor fit to the regression line. Small taxa like *Hyrachyus*, *Hyracodon* and small Elasmotheriinae plot above the regression line together with *Metamynodon*, some Aceratheriini and Rhinocerotina. *Paraceratherium* plots far above the regression line. Teleoceratina are all grouped below the line together with most of Rhinocerotina (Fig. 5A). Hyrachyidae, Hyracodontidae, Amynodontidae and Paraceratheriidae seem to follow an independent path parallel to that of Rhinocerotidae one, but as these groups have few representatives here, this observation must be taken with caution. Changes in CS values mainly affect the general robustness of the bone, which is slightly increased in larger femora. It also affects the greater trochanter tuberosity and convexity, the femoral head and particularly the fovea capitis. Along the shaft, the main changes are located on the lateral part between the greater trochanter convexity and the third trochanter (where inserts the m. vastus lateralis), as well as along the distal half of the diaphysis, on the cranial and caudal sides. Lateral and medial parts of both condyles are also strongly modified by CS variations (Fig. 5A; Supporting Information, Fig. S3A).

Table 3. Range of R^2 and *P*-values for PGLS computed with NNI permuted trees on shape data and log-transformed centroid size (CS), log-transformed cubic root of mean body mass (BM) and log-transformed mean gracility index (GI-MT3). *N*: number of trees obtained after NNI procedure; R^2: determination coefficient value. Significant results (for mean $P < 0.01$) are indicated in bold

Bone	Variable	*N*	R^2			*P*-value		
			Min.	Max.	Mean	Min.	Max.	Mean
Femur (complete)	**CS**	**76**	**0.06**	**0.10**	**0.07**	**0.001**	**0.022**	**0.003**
	BM	**46**	**0.14**	**0.23**	**0.16**	**0.001**	**0.005**	**0.002**
	GI	**74**	**0.06**	**0.07**	**0.09**	**0.001**	**0.011**	**0.003**
Femur (proximal partial)	**CS**	**80**	**0.05**	**0.11**	**0.07**	**0.001**	**0.015**	**0.004**
	BM	**48**	**0.08**	**0.11**	**0.11**	**0.001**	**0.016**	**0.002**
	GI	**78**	**0.05**	**0.07**	**0.06**	**0.001**	**0.030**	**0.009**
Femur (distal partial)	CS	86	0.06	0.07	0.06	0.017	0.051	0.033
	BM	52	0.07	0.10	0.08	0.042	0.182	0.095
	GI	**82**	**0.06**	**0.08**	**0.07**	**0.002**	**0.025**	**0.011**
Tibia	CS	82	0.04	0.06	0.04	0.040	0.119	0.082
	BM	**52**	**0.08**	**0.18**	**0.13**	**0.004**	**0.048**	**0.009**
	GI	**80**	**0.22**	**0.31**	**0.27**	**0.001**	**0.001**	**0.001**
Fibula	CS	52	0.05	0.10	0.08	0.018	0.267	0.046
	BM	42	0.03	0.11	0.08	0.051	0.0.597	0.146
	GI	**50**	**0.17**	**0.22**	**0.20**	**0.001**	**0.003**	**0.001**

The structure of the regression plot of shape against BM is partly similar to that obtained with CS, with a relatively poor fit to the regression line, mainly driven by *Hyrachyus* at the minimal BM values. *Hyrachyus* is clearly isolated from all other species that form a large cluster at high BM values (Fig. 5B). *Metamynodon* (Amynodontidae) plots outside this cluster and far above from the regression line. A variation of BM results in the modifications of the same anatomical areas as for CS, although to a stronger extent, particularly for the femoral head and the greater trochanter convexity. An increase of robustness is observed towards high BM values. Shape changes are also located along the lesser trochanter, the medial lip of the trochlea and the medial epicondyle (Fig. 5B; Supporting Information, Fig. S3B). The regression plot of shape against GI-MT3 indicates a good fit to the regression line, better than those with CS and BM. We can observe a clear separation between Rhinocerotina, being almost all above the regression line at mid-GI-MT3 values and most other species below the line at various GI-MT3 values. Hyrachyidae and Hyracodontidae isolated towards minimal values, together with *Menoceras* Troxell, 1921, while other small Elasmotheriinae group with *Paraceratherium*, *Trigonias* and some gracile Aceratheriini and Rhinocerotina. Teleoceratina form a homogeneous cluster slightly isolated from other species (Fig. 5C). As for BM and CS, variations of GI-MT3 are associated with changes in bone robustness, but are also related to modifications located on both medial and lateral supracondylar areas where inserts the m. gastrocnemius. However, contrary to what is observed with BM, the medial lip of the trochlea and the medial epicondyle are poorly modified with variations of GI-MT3 values (Fig. 5C; Supporting Information, Fig. S3C).

Femur—proximal part

Shape data for the proximal part of the femur carry a significant phylogenetic signal ($K_{mult} = 0.62$, $P < 0.01$). The distribution of the species in the NJ tree (Fig. 3B) and in the phylomorphospace (Fig. 6A) shows marked differences with the results obtained on complete bones. The NJ tree is structured by separation into three main clusters: (1) Hyrachyidae, Hyracodontidae, small Elasmotheriinae together with one rhinocerotine *incertae sedis* (*i.s.*) (*Protaceratherium*) and one aceratheriine (*Pe. profectum*); (2) almost all Rhinocerotina together with *Pleuroceros*; and (3) Aceratheriini, Teleoceratina and Paraceratheriidae, together with *Metamynodon* and *Trigonias*. A similar structure is observed in the phylomorphospace, where the two first axes carry 62.1% of the total variance. PC1, which gathers 42.2% of the variance, mainly highlights the opposition between giant Paraceratheriidae on positive values and Rhinocerotina on negative values. PC2 gathers 19.9% of the variance and mainly separates small taxa (*Hyrachyus*, *Hyracodon*, small Elasmotheriinae, *Protaceratherium*, *Pe. profectum*) towards negative values from all other species towards positive values. *Metamynodon* and *Aphelops*

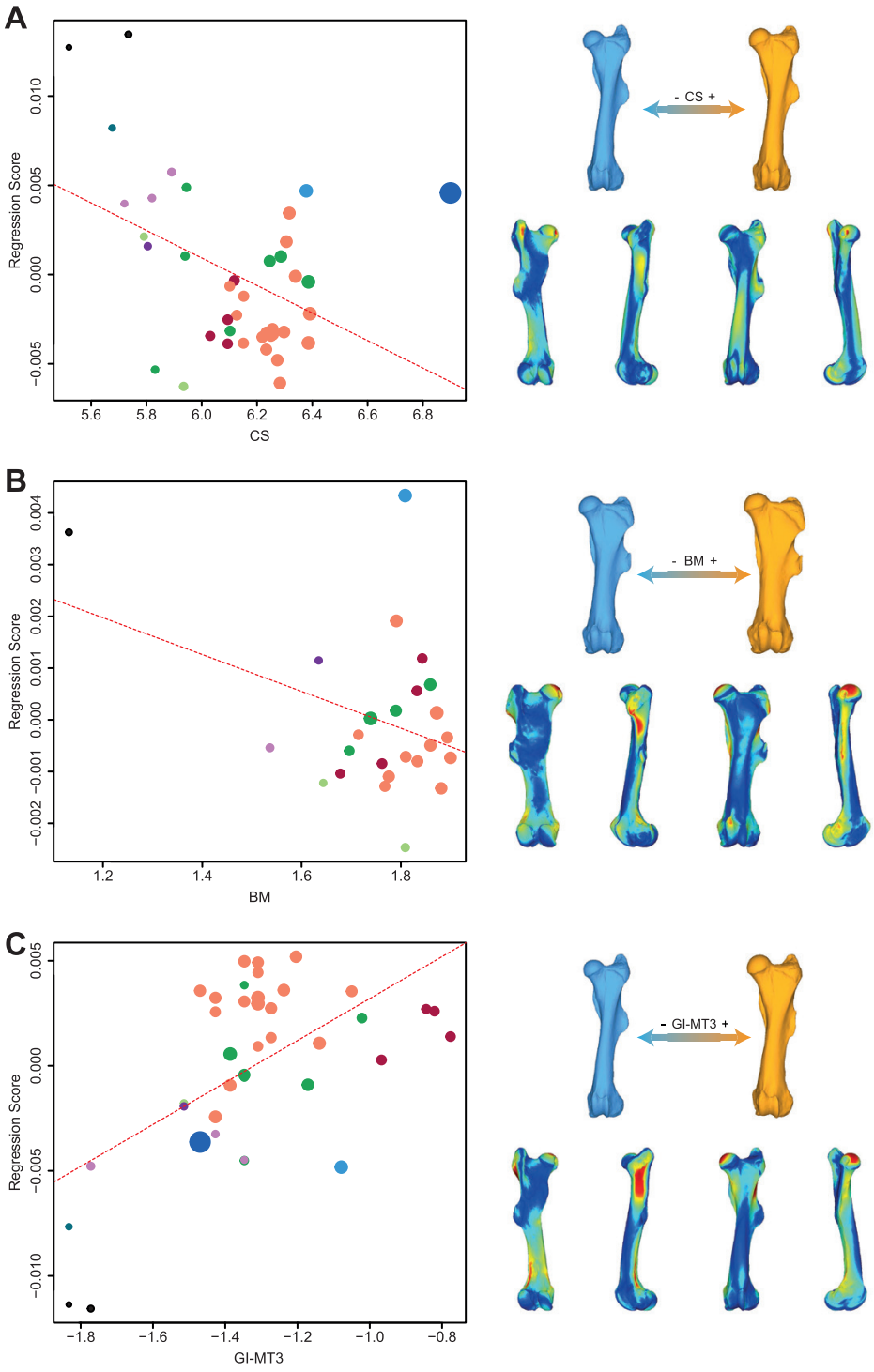

Figure 5. Significant PGLS regression plots for complete femur performed on shape data and log-transformed centroid size (CS) (A), log-transformed cubic root of mean body mass (BM) (B), log-transformed mean gracility index (GI-MT3) (C). Point colour code follows Figure 1. Point size is proportional to mean log CS of each species. On the right, shapes associated with minimum and maximum fitted values (top row) and colour maps of the location and intensity of the shape deformation (bottom row). Blue: minimum value of the regression. Orange: maximum value of the regression. For each bone, the shape associated with the minimum was coloured depending on its distance to the shape associated with the maximum (blue indicates a low deformation intensity and red indicates a high deformation intensity). Orientation from left to right in each case: caudal, lateral, cranial and medial.

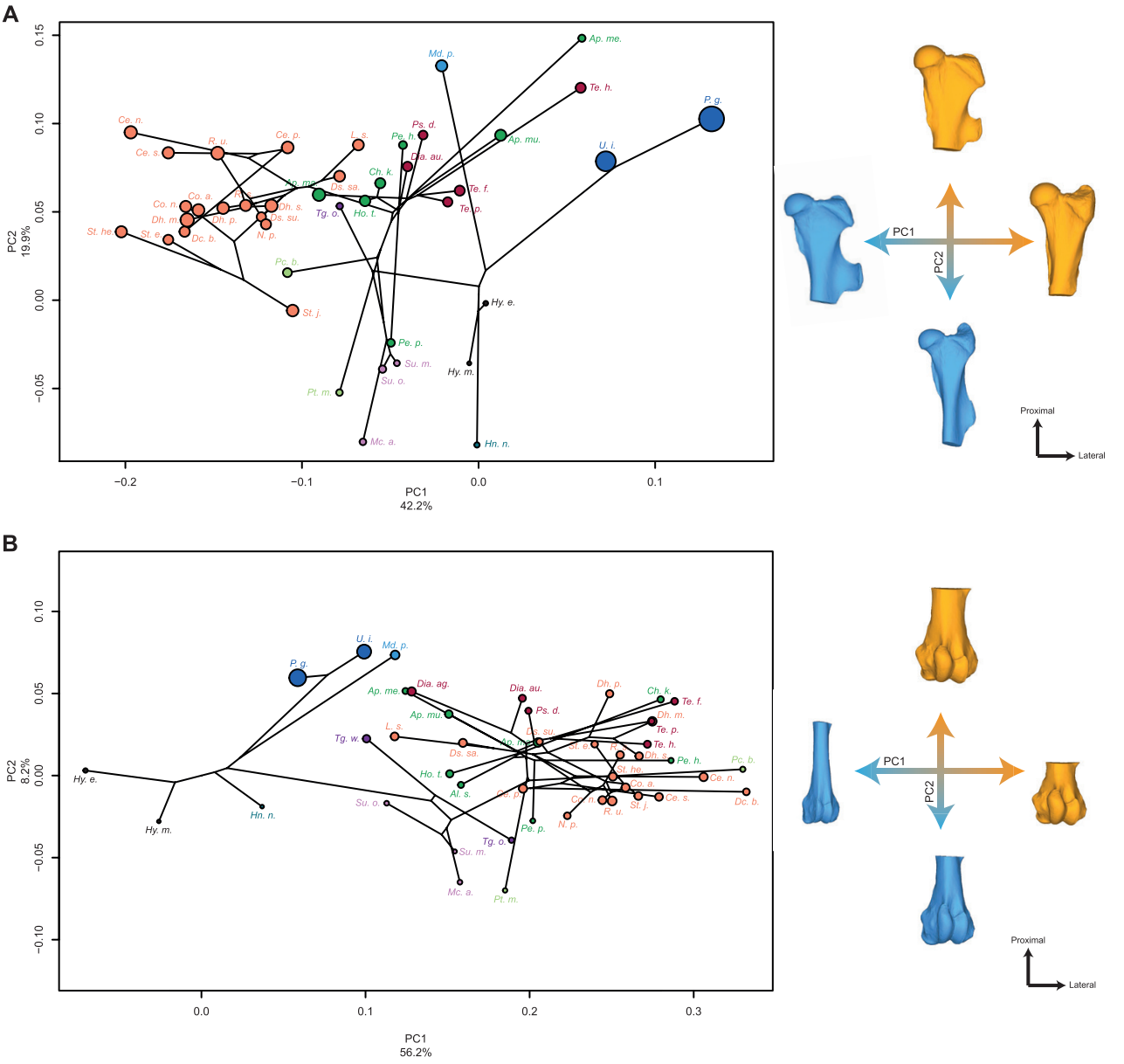

Figure 6. Results of the PCA performed on morphometric data of proximal partial femur (A) and distal partial femur (B) and shape variation associated with the first two axes of the PCA (caudal view). Blue: negative side of the axis. Orange: positive side of the axis. Phylogenetic relationships are plotted in the morphospace. Colour codes follow Figure 1 and abbreviations follow Table 1. Point size is proportional to the mean log centroid size of each species.

megalodus occupy the highest positive values along this axis.

Along PC1, shape variation is mostly related to the general orientation of the proximal part relative to the rest of the bone and the development and position of the trochanters (Fig. 6A; Supporting Information, Fig. S2B). Towards negative values, the proximal part of the femur is tilted medially, with a relatively flattened head; a poorly developed greater trochanter tuberosity; a lesser trochanter placed directly below the femoral neck and above the third trochanter along the shaft; and a third trochanter strongly extended cranially and laterally. Towards positive values, the proximal part of the femur is more vertical, with a rounded head supported by a thick neck; a greater trochanter tuberosity developed proximally and caudally; a long lesser trochanter situated in front of the third trochanter along the shaft; and a third trochanter almost absent and reduced to a bony rugosity. Along PC2, the shape associated with negative values

is long and slender, with a rounded head oriented proximomedially; a high greater trochanter tuberosity; a short lesser trochanter; and a long and poorly laterally developed third trochanter. The shape associated with positive values shows a flattened head oriented proximally; a low greater trochanter tuberosity; a long lesser trochanter; and a third trochanter developed laterally and cranially.

As for the complete bones, CS of the proximal femur carries a strong phylogenetic signal (K_{CS} = 1.86, P < 0.01) and is strongly correlated with BM (r = 0.91, P < 0.01) but not with GI-MT3 (P = 0.18) (Table 2). Similarly, PGLS regressions indicate a significant correlation between shape and the three variables. The NNI procedure highlights that some phylogenetic uncertainties can lead to marginally non-significant results (Table 3). The regression plot of shape against CS displays a poor fit to the regression line, with a high dispersion of specimens. Almost all Rhinocerotina are below the regression line, only associated with Rhinocerotinae *i.s.*, *Trigonias*, *Subhyracodon* (Elasmotheriinae) and *Aphelops* (Aceratheriini). Above the regression line, Aceratheriini and Teleoceratina group together with *Metamynodon* (Amynodontidae), while Hyrachyidae and Hyracodontidae also plot well above the line at low CS values. Giant Paraceratheriidae plot far above the regression line at high CS values. They do not seem to follow the same allometric trend as other rhinocerotoids in the present case, and their presence probably pulled the regression line upwards at high CS values (Fig. 7A). The regression plot of shape against BM also displays a relatively poor fit to the regression line. *Hyrachyus* and *Paraceratherium* are isolated from most other taxa at extreme CS values and plot far above the regression line. Again, almost all Rhinocerotina situated below the line are separated from other species situated above the line (Fig. 7B). Contrary to the results obtained on complete bones, the regression plot of shape against GI-MT3 shows a more scattered dispersion of the species. There is also no clear preferential direction shown by the overall distribution of all specimens, which highlights a relatively poor fit to the regression line. As for CS and BM, Rhinocerotina clearly isolate on one side of the regression line (above in this case), while almost all other species plot on the other side [far below for Paraceratheriidae, Hyrachyidae and *Teleoceras proterum* (Leidy, 1885)] (Fig. 7C). As for complete bones, shape variation associated with changes in CS and BM values impacts similar anatomical areas: mainly the greater trochanter tuberosity, the lesser trochanter and the cranial side of the shaft. However, the increase of robustness towards high values is not clear. The intensity of shape variation is slightly higher for BM than CS (Fig. 7A, B; Supporting Information, Fig. S3D, E). The shape changes associated with variations of GI-MT3 values mainly concern the femoral head, the lesser and third trochanters and the insertion area of the m. vastus lateralis (Fig. 7C; Supporting Information, Fig. S3F).

Femur—distal part

The phylogenetic signal carried by shape data for the distal part of the femur is strong and significant (K_{mult} = 1.06, P < 0.01). The distribution of the species in the NJ tree (Fig. 3C) and in the phylomorphospace (Fig. 6B) differs noticeably from those obtained on the complete bone and proximal part. The NJ tree depicts an opposition between gracile and brachypodial taxa, with a poor influence of phylogenetic relationships: only Rhinocerotina group almost all together, despite the presence of Aceratheriini and Teleoceratina close to them. This sorting along the degree of brachypody is also observed on the phylomorphospace (especially PC1), where the first two axes gather 64.4% of the global variance (Fig. 6B). Along PC1, which carries 56.2% of the variance, *Hyrachyus* and *Hyracodon* plot together around null values, close to giant Paraceratheriidae and *Metamynodon*. Small Elasmotheriinae, *Trigonias* and *Protaceratherium* are mixed with relatively gracile Aceratheriini, Rhinocerotina and Teleoceratina, while the most brachypodial taxa (*Teleoceras*, *Chilotherium*, *Pleuroceros*) plot towards the maximal positive values, together with some *Dihoplus* Brandt, 1878, *Ceratotherium* Gray, 1868 and *Diceros* Gray, 1821. PC2, which gathers 8.2% of the variance, mainly opposes small Elasmotheriinae and *Protaceratherium* towards negative values to giant Paraceratheriidae and *Metamynodon* towards positive values. However, no clear pattern is visible regarding other taxa between these two extremes.

As for complete bones, shape variation along PC1 is mainly related to the general robustness of the bone (Fig. 6B; Supporting Information, Fig. S2C). Theoretical shape associated with negative values displays a long and slender shaft; a narrow symmetrical trochlea developing caudally towards the condyles; symmetrical medial and lateral condyles. Conversely, the shape associated with positive values shows a robust and thick shaft, compressed proximodistally; an asymmetrical trochlea with a massive medial lip; a medial condyle more developed than the lateral one; and a protruding medial epicondyle. Along PC2, the shape associated with negative values has a narrower shaft; a medial lip of the trochlea poorly developed in the cranial direction; a narrow and deep V-profiled trochlear groove; and medial and lateral condyles developed in the caudal direction. Conversely, the shape associated with positive values shows a more robust shaft; a medial lip of the trochlea which is more developed in the cranial direction; a wide and shallow

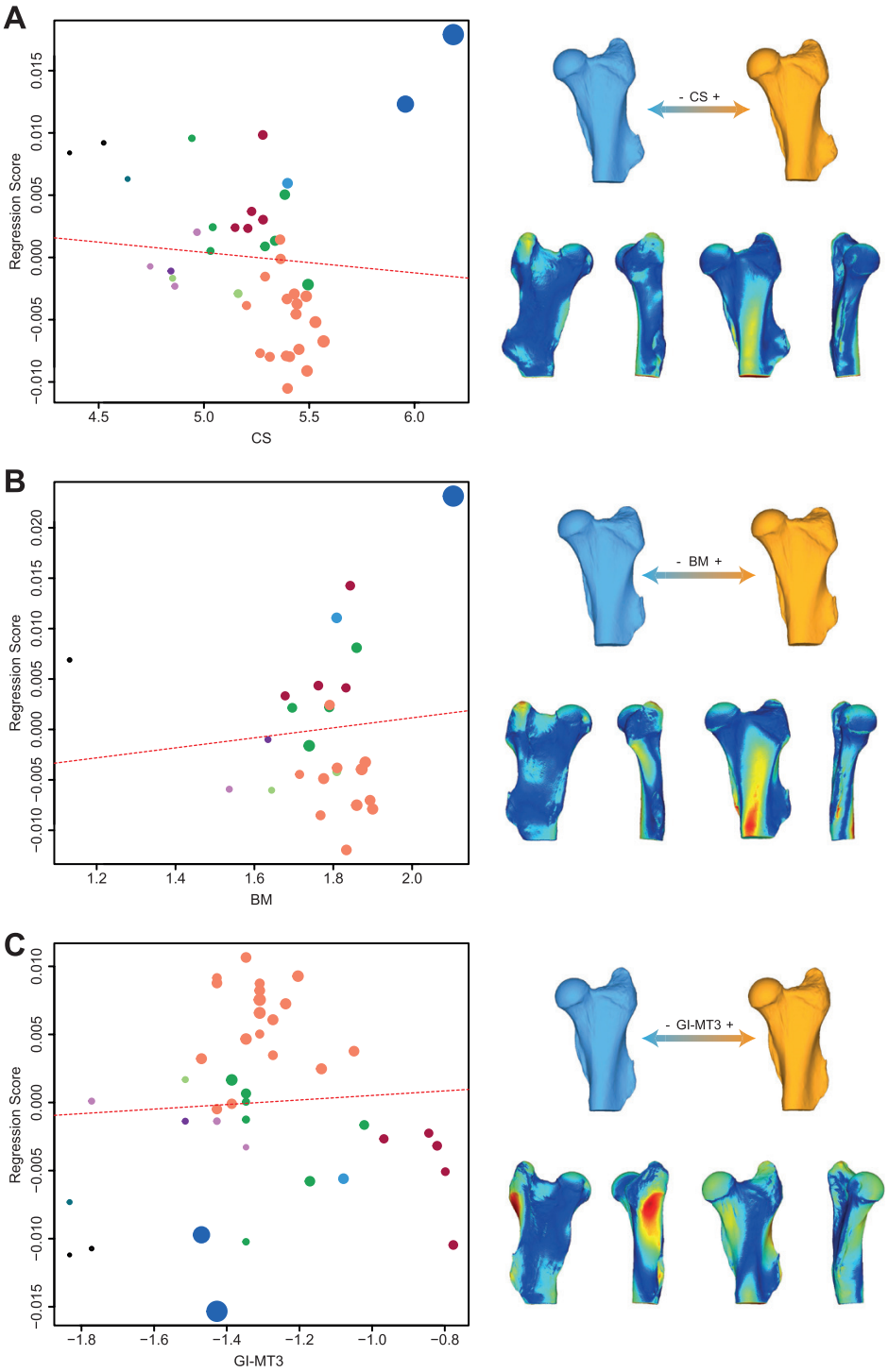

Figure 7. Significant PGLS regression plots for proximal partial femur performed on shape data and log-transformed centroid size (CS) (A), log-transformed cubic root of mean body mass (BM) (B), log-transformed mean gracility index (GI-MT3) (C). Point colour code follows Figure 1. Point size is proportional to mean log CS of each species. On the right, shapes associated with minimum and maximum fitted values (top row) and colour maps of the location and intensity of the shape deformation (bottom row). Blue: minimum value of the regression. Orange: maximum value of the regression. For each bone, the shape associated with the minimum was coloured depending on its distance to the shape associated with the maximum (blue indicates a low deformation intensity and red indicates a high deformation intensity). Orientation from left to right in each case: caudal, lateral, cranial and medial.

trochlear groove; and medial and lateral condyles which are poorly developed in the caudal direction.

The centroid size of the distal femur carries a significant phylogenetic signal (K_{CS} = 0.91, P < 0.01) and is highly correlated with BM (r = 0.86, P < 0.01) but not with GI-MT3 (P = 0.32) (Table 2). However, contrary to what is observed on the complete bone and proximal part, PGLS regressions are only significant between shape and GI-MT3 (and marginally between shape and CS depending on the tree configuration) (Table 3). The regression plot of shape against GI-MT3 is similar to that observed on the complete femur and shows a relatively good fit to the regression line (Fig. 8). Almost all Rhinocerotina are above the regression line, together with *Trigonias*, *Protaceratherium* and *Menoceras*. Aceratheriini are dispersed on each side of the line, some being mixed with Rhinocerotina. Below the regression line, Teleoceratina are grouped together with Paraceratheriidae and *Metamynodon*, while Hyrachyidae and Hyracodontidae isolate below the line towards minimal GI-MT3 values (Fig. 8). As for complete bones, beyond a slight increase of robustness, the shape variation associated with variations of GI-MT3 values is mainly located on both medial and lateral supracondylar areas where inserts the m. gastrocnemius (Fig. 8; Supporting Information, Fig. S3G). Although marginally non-significant, the regression plot of shape against CS displays a strong similarity with those obtained on the complete bone and proximal part, with a relatively weak fit to the regression line. We observe an opposition between almost all Rhinocerotina and Teleoceratina below the regression line (together with Rhinocerotinae *i.s.*) and all other species above the line. As in previous results, Aceratheriini are dispersed among this central cluster, while *Hyrachyus-Hyracodon* and giant Paraceratheriidae plot far away from the line at minimal and maximal CS values, respectively. Similarly, shape variation associated with changes of CS values mainly affects the third trochanter, the cranial side of the shaft and both medial and lateral condyles [see Supporting Information (Fig. S4A) for regression plot and shape deformation].

Tibia

As was observed for the femur, shape data obtained on the tibia carry a significant phylogenetic signal (K_{mult} = 1.27, P < 0.01). The NJ tree is strongly structured by the degree of brachypody, opposing mainly Hyrachyidae to the most brachypodial species of Teleoceratina (Fig. 3D). Rhinocerotina plot almost all together. *Elasmotherium* and *Diaceratherium* Dietrich, 1931 plot within the Aceratheriini group, whereas all other Teleoceratina are isolated at an extremity of the tree. *Paraceratherium* is close to *Peraceras* Cope, 1880 and some Rhinocerotina, but also of all other Aceratheriini. The first two axes of the phylomorphospace gather 78.0% of the total variance and display a structure similar to that of the NJ tree (Fig. 9A). PC1 carries 65.4% of the variance and is associated with bone robustness, with gracile tibiae occupying positive values and robust tibiae negative values. PC1 opposes Hyrachyidae and Hyracodontidae towards positive values to Teleoceratina towards negative values. Along this axis, small Elasmotheriinae plot next to Hyrachyidae and Hyracodontidae, together with *Protaceratherium*. Species with a larger tibia like *Elasmotherium* and *Paraceratherium* plot together with most of the Aceratheriini, the genus *Diaceratherium* and some Rhinocerotina. Taxa with a short and robust tibia like *Teleoceras*, *Brachypotherium* Roger, 1904, *Prosantorhinus* Heissig, 1973 and *Pleuroceros* occupy the most negative values. PC2 carries 12.6% of the variance and mainly opposes Teleoceratina with a short and robust tibia towards negative values to some Rhinocerotina (with gracile tibia like *Stephanorhinus* Kretzoi, 1942, *Dicerorhinus* Gloger, 1841 and more robust ones like *Ceratotherium* and *Dihoplus*), as well as *Pe. profectum* and *Paraceratherium* towards positive values.

Shape variation along PC1 is mostly related to the general robustness of the bone (Fig. 9A; Supporting Information, Fig. S2D). Towards positive values, the tibia is thin and slender, with: a triangular tibial plateau tilted in the caudal direction and showing similar surface areas for the medial and lateral articular surfaces; a lateral surface area highly developed in the caudal direction towards the popliteal notch; medial and lateral intercondylar tubercles separated by a large gap; a small and flat tibial tuberosity associated with a narrow and deep tibial groove; a long and narrow shaft with relatively parallel medial and lateral edges; a distal articular surface for the fibula forming an isosceles triangle; a narrow and asymmetrical articular surface for the astragalus, with a lateral groove deeper than the medial one; and a caudal apophysis stretched caudally. Conversely, the theoretical shape associated with negative values is highly robust and thick, with: an irregular tibial plateau tilted medially and cranially; a medial articular surface wider than the lateral one; a lateral surface area poorly developed in the caudal direction towards the popliteal notch; medial and lateral intercondylar tubercles separated by a narrow gap; a strong and massive tibial tuberosity oriented laterally and associated with a wide and shallow tibial groove; a massive diaphysis displaying a narrowing at midshaft, conferring to the bone an hourglass aspect in cranial view; a distal articular surface for the fibula forming an equilateral triangle; and a wide, shallow and relatively symmetrical articular surface for the astragalus. Along PC2, shape variation mainly

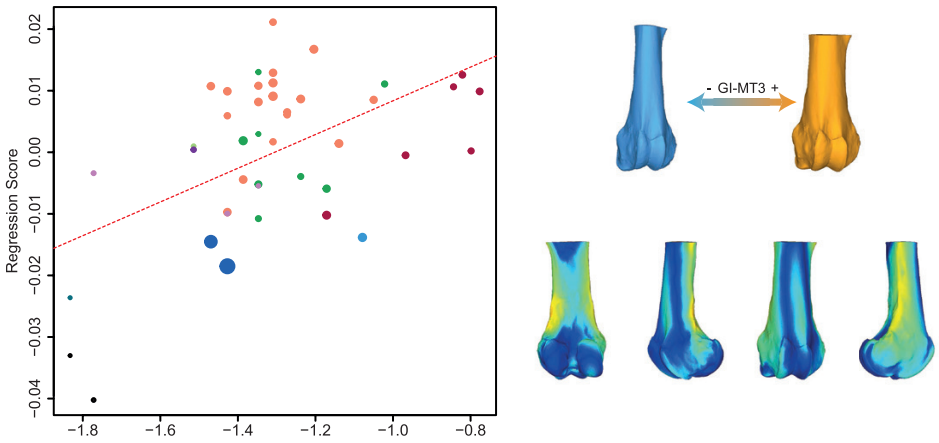

Figure 8. Significant PGLS regression plot for distal partial femur performed on shape data and log-transformed mean gracility index (GI-MT3). Point colour code follows Figure 1. Point size is proportional to mean log CS of each species. On the right, shapes associated with minimum and maximum fitted values (top row) and colour maps of the location and intensity of the shape deformation (bottom row). Blue: minimum value of the regression. Orange: maximum value of the regression. For each bone, the shape associated with the minimum was coloured depending on its distance to the shape associated with the maximum (blue indicates a low deformation intensity and red indicates a high deformation intensity). Orientation from left to right: caudal, lateral, cranial and medial.

affects both epiphyses. Towards positive values, the tibia has high intercondylar tubercles, with the medial one being placed more cranially than the lateral one; both medial and lateral condyles being developed caudally defining a deep popliteal notch; a high tibial tuberosity; a straight interosseous crest; a long distal articular surface for the fibula forming an isosceles triangle; a symmetrical articular surface for the astragalus; and a medial malleolus developed distally. Conversely, towards negative values, the tibia has low intercondylar tubercles, both facing each other; medial and lateral condyles poorly developed caudally resulting in a narrow popliteal notch; a low tibial tuberosity; a rounded and concave interosseous crest; a short kidney-shaped distal articular surface for the fibula; an articular surface for the astragalus with a craniocaudally tilted general axis; and a medial malleolus poorly developed distally.

The centroid size of the tibia carries a significant although weak phylogenetic signal relative to the results obtained on the femur (K_{CS} = 0.56, P = 0.01). Similarly, CS is strongly correlated with BM (r = 0.72, P < 0.01) but not with GI-MT3 (P = 0.14) (Table 2). PGLS regressions are significant for BM and GI-MT3 only, although the NNI procedure indicates that some tree configurations may led to significant results for CS as well (Table 3). The regression plot of shape against BM shares strong similarities with that obtained on the femur. Specimens show a rather good fit to the regression line with few outliers. Towards high BM values, there is a high dispersion of the species and a strong opposition between large Paraceratheriidae and some Teleoceratina on each side of the line. Conversely, Elasmotheriinae follow a trend parallel to the common regression line (Fig. 10A). The shape variation associated with changes of BM values is mostly located directly under the tibial plateau on the medial and lateral sides of the shaft, with a stronger intensity of shape variation in the former location. The tibial crest is also affected by shape changes of lesser intensity. The medial side of the tibial shaft is particularly affected by shape changes, especially proximally (Fig. 10A; Supporting Information, Fig. S3H). The regression plot of shape against GI-MT3 shows a good fit to the regression line. This plot is similar to that obtained on the femur, with the isolation of almost all Rhinocerotina above the regression line, only associated with *Elasmotherium*, *Paraceratherium* and *Aphelops*. Below the regression line, Hyrachyidae-Hyracodontidae, small Elasmotheriinae, Aceratheriini and Teleoceratina all form homogeneous groups separated from each other along GI-MT3 values (Fig. 10B). Towards high values of GI-MT3, shape variation involves an increase of robustness and a mediolateral broadening of both epiphyses (Fig. 10B; Supporting Information, Fig. S3I). Shape variation is similar to that observed for changes in BM values, with a stronger general robustness and marked anatomical modifications located under the tibial plateau. These changes are mainly located on the proximal part of the medial side of the tibia, and distally to the tibial tuberosity. The distal part of the shaft is also affected, notably the distal articular surface for the fibula [see Supporting Information (Fig. S3) for shape deformation].

FIBULA

The results obtained on the fibula differ strongly from those obtained on previous bones. Although significant, the phylogenetic signal carried by shape data is almost equal to 1 ($K_{mult} = 0.99, P < 0.01$), indicating a negligible influence of phylogenetic relations on the shape of the fibula. The distribution of the species on the NJ tree (Fig. 3E) and on the phylomorphospace (Fig. 9B) strongly differs from those obtained for the femur and the tibia. The NJ tree is mainly structured by an opposition between Teleoceratina, *Hyrachyus* and *Menoceras* on the one hand and Rhinocerotinae *i.s.*, Aceratheriini, Paraceratheriidae and Rhinocerotina strongly mixed together on the other hand. The first two axes of the phylomorphospace, gathering 76.0% of the global variance, reflect a similar structure to the NJ tree (Fig. 9B). PC1, accounting for 47.2% of the variance, opposes *Hyrachyus*, *Menoceras* and almost all Teleoceratina in the negative part to all other species on the positive part. Rhinocerotina, Aceratheriini and Rhinocerotinae *i.s.* form a cluster

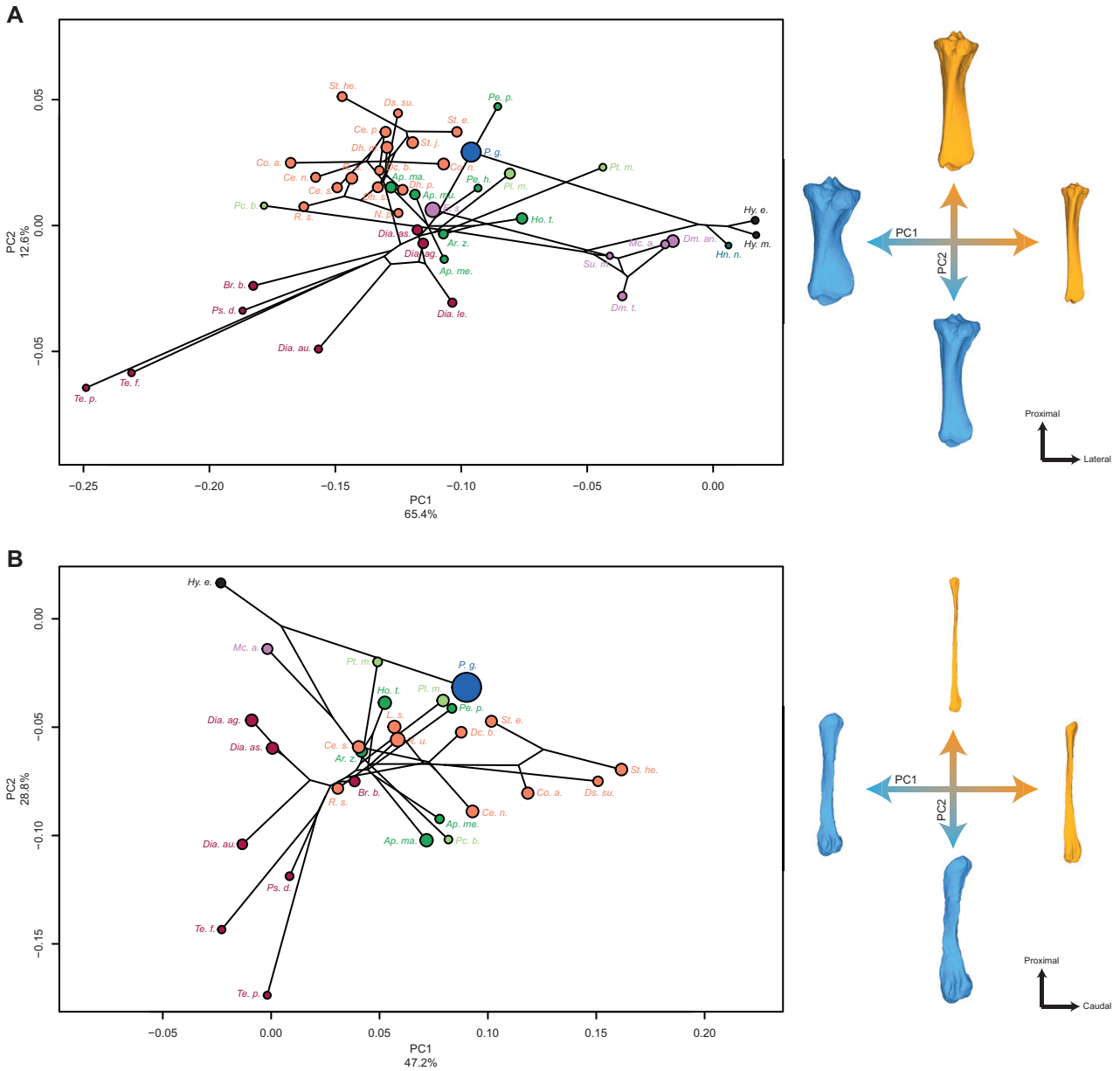

Figure 9. Results of the PCA performed on morphometric data of tibia (A) and fibula (B) and shape variation associated with the first two axes of the PCA (caudal view). Blue: negative side of the axis. Orange: positive side of the axis. Phylogenetic relationships are plotted in the morphospace. Colour codes follow Figure 1 and abbreviations follow Table 1. Point size is proportional to the mean log centroid size of each species.

with no obvious structure. *Paraceratherium* plots near small taxa like *Protaceratherium* and *Peraceras*, but also near *Pleuroceros* and *Aphelops*. PC2, which gathers 28.8% of the variance, is mainly driven by an opposition between *Hyrachyus* and *Menoceras* towards positive values and *Teleoceras* towards negative values. Along this axis, while Rhinocerotina plot mainly with Teleoceratina, *Paraceratherium* is close to small taxa like *Menoceras*, *Plesiaceratherium* Young, 1937 and *Protaceratherium*. Aceratheriini are mixed together with Rhinocerotinae *i.s.*, Rhinocerotina and poorly brachypodial Teleoceratina.

Contrary to what was observed for the femur and the tibia, the shape variation along PC1 is less related to a change in the general robustness of the bone than along PC2 (Fig. 9B; Supporting Information, Fig. S2E). The shape associated with positive values is thin with a small rounded proximal articular surface for the tibia oriented cranially; a thin central shaft with a sharp interosseous crest; a long distal articular surface for the tibia forming an isosceles triangle; a mediolaterally flattened distal epiphysis; both cranial and caudal tubercles of the lateral malleolus being oriented caudally; and a symmetrical kidney-shaped articular surface for the astragalus. Conversely, the shape associated with negative values is massive and thick with a large proximal articular surface for the tibia oriented more medially; a strong central shaft with a smooth interosseous crest; a short distal articular surface for the tibia forming an equilateral triangle; a mediolaterally broadened distal epiphysis; both cranial and caudal tubercles of the lateral malleolus oriented laterally; and an asymmetrical kidney-shaped articular surface for the astragalus. Surprisingly, shape variation along PC2 also involves a huge change in robustness more marked than along PC1 and associated with morphological changes of both epiphyses. The shape associated with positive values is extremely thin and flat, with a spoon-like proximal articular surface for the tibia; a straight and flat shaft; a distal epiphysis with a caudal development conferring it a squared shape; and a small rectangular articular surface for the astragalus. The shape associated with negative values is extremely thick and massive with a large proximal articular surface for the tibia; a strong shaft with a craniocaudal curvature; a triangular and thick distal epiphysis; and a kidney-shaped articular surface for the astragalus.

Contrary to what is observed in other bones, the centroid size of the fibula does not carry a significant phylogenetic signal ($P = 0.22$). CS is highly correlated with BM ($r = 0.71$, $P < 0.01$), but not with GI-MT3 ($P = 0.17$) (Table 2). As for the distal femur, PGLS regressions are only significant between shape and GI-MT3 (and marginally between shape and CS depending on the tree configuration) (Table 3). However, the regression plot of shape against GI-MT3 indicates a poor fit to the regression line, with many species plotting far away from the line (Fig. 10C). Rhinocerotina are almost all grouped above the regression line at mid-GI-MT3 values, while Teleoceratina are grouped below the line at high GI-MT3 values. Aceratheriini plot near Rhinocerotinae *i.s.* and *Paraceratherium* in the central cluster while *Hyrachyus* (Hyrachyidae) and *Menoceras* (Elasmotheriinae) isolate towards minimal GI-MT3 values, well below the line. The shape variation associated with changes of GI-MT3 values mainly involves morphological modifications of the caudal side of the fibula head, of the lateral part of the shaft and of the distal epiphysis, particularly the cranial and caudal tubercles of the malleolus and the distal articular surface for the tibia (Fig. 10C; Supporting Information, Fig. S3J). PGLS regression between shape and CS is non-significant at the considered threshold of $P < 0.01$ (Table 3). The regression plot indicates a weak fit to the regression line. *Paraceratherium* appears to strongly drive the regression trend being the only taxon with high CS values [see Supporting Information (Fig. S4B) for regression plot]. The shape variation associated with a higher CS involves mainly the same anatomical areas as those described for the shape variation related to GI-MT3 [see Supporting Information (Fig. S4B) for shape deformation].

Evolution of CS values along the phylogeny

The evolution of CS values along the phylogeny for the distal femur (being that with the least amount of missing data), complete tibia and complete fibula (Fig. 11) highlights important disparities between the three bones. The distribution of CS values for the tibia is particularly distinct from those observed on the femur and the fibula. This distinction is notably due to Teleoceratina, showing low values of CS for the tibia. On the fibula, the lowest values are not represented by *Hyrachyus* but by *Teleoceras*. Despite missing taxa for the fibula, most CS values for other taxa seem congruent with the distribution observed for the distal femur.

DISCUSSION

Association of mass, size and gracility with bone shape

Congruent shape variation associated with all variables

While it is never significantly correlated either with CS or BM, the gracility index GI-MT3 is always significantly correlated with shape variation for the femur, tibia and fibula. CS is always significantly and

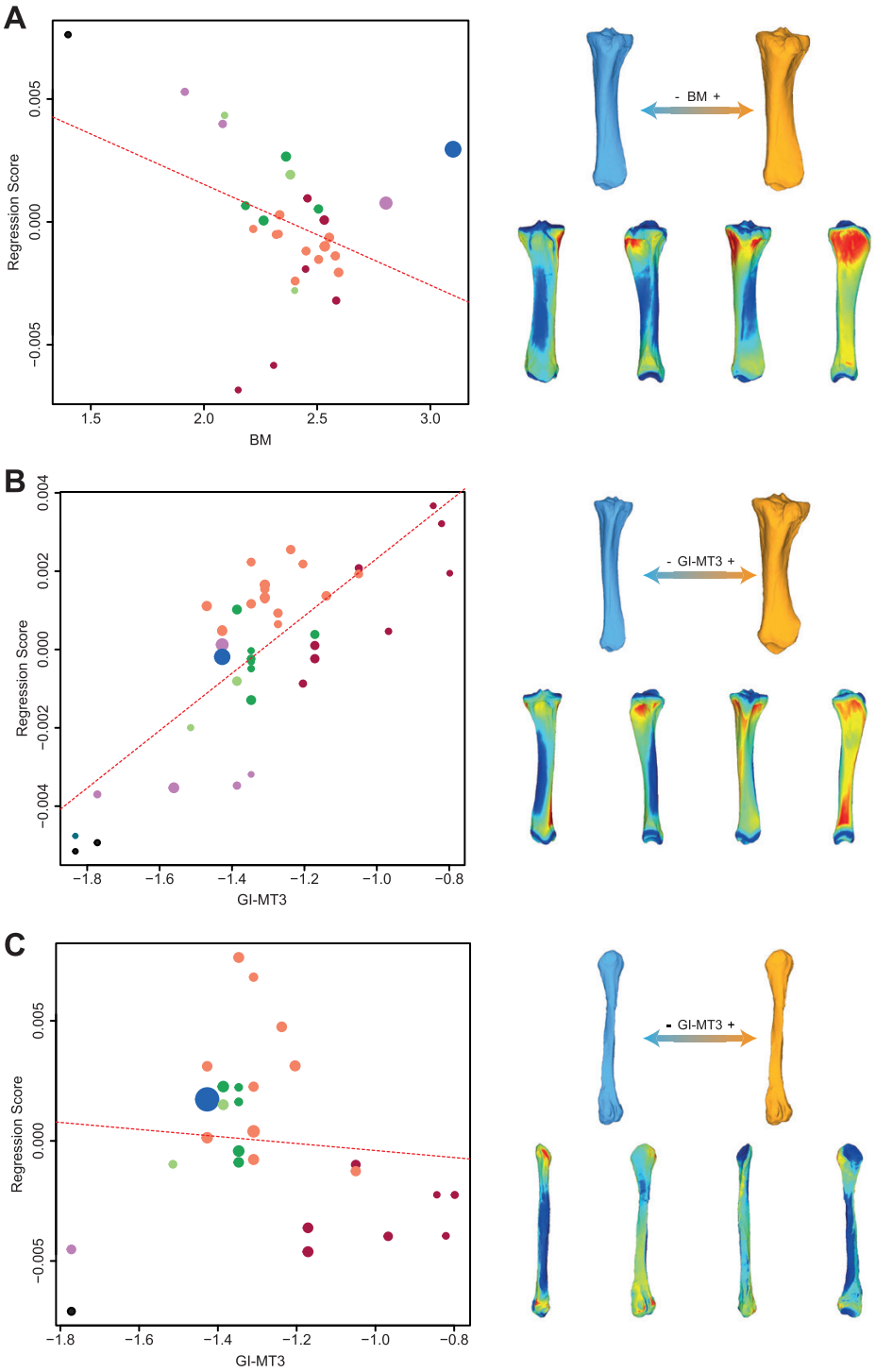

Figure 10. Significant PGLS regression plots for tibia performed on shape data and log-transformed cubic root of mean body mass (BM) (A), log-transformed mean gracility index (GI-MT3) (B), and fibula performed on shape data and log-transformed mean gracility index (GI-MT3) (C). Point colour code follows Figure 1. Point size is proportional to mean log CS of each species. On the right, shapes associated with minimum and maximum fitted values (top row) and colour maps of the location and intensity of the shape deformation (bottom row). Blue: minimum value of the regression. Orange: maximum value of the regression. For each bone, the shape associated with the minimum was coloured depending on its distance to the shape associated with the maximum (blue indicates a low deformation intensity and red indicates a high deformation intensity). Orientation from left to right in each case: caudal, lateral, cranial and medial.

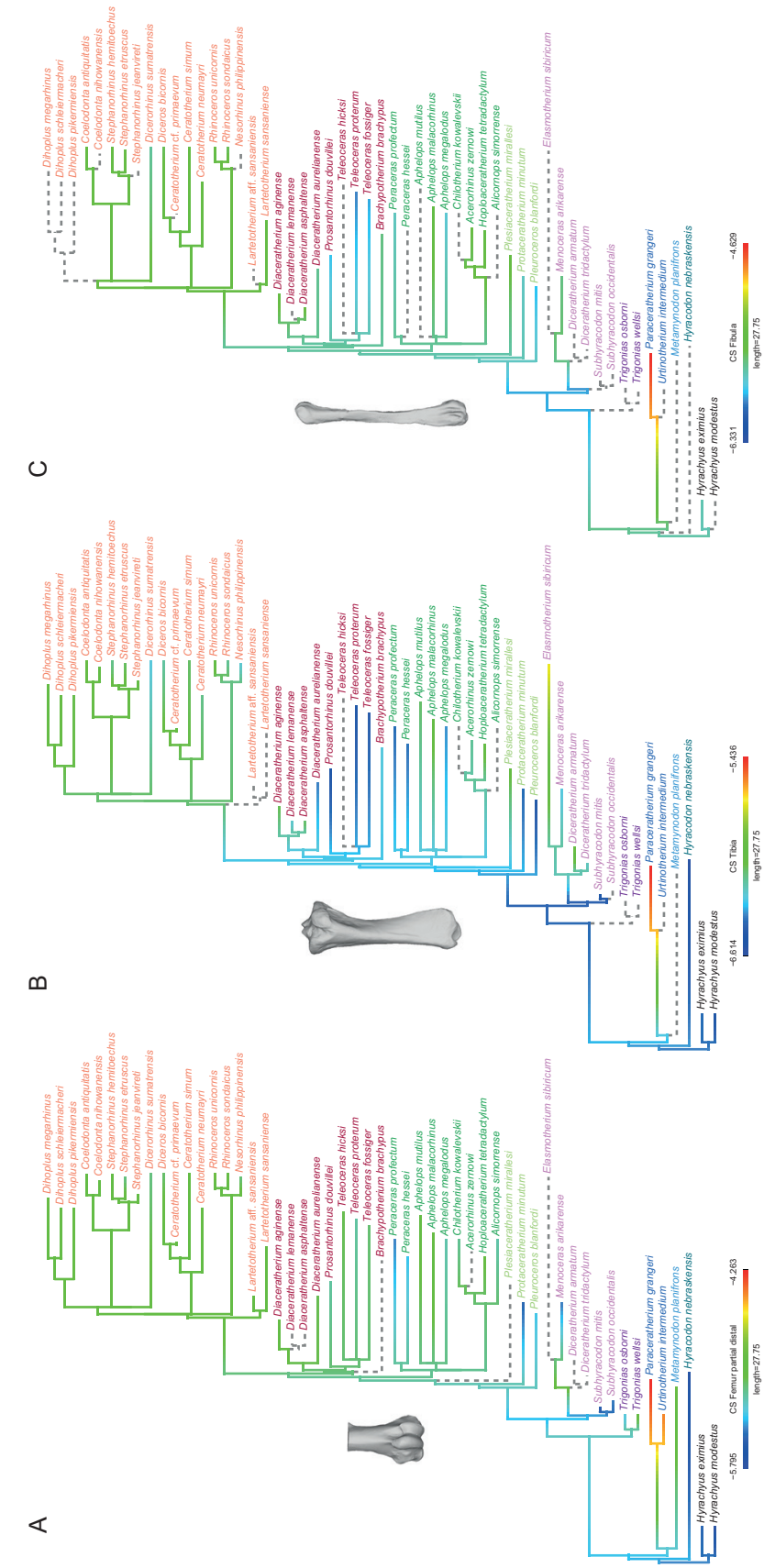

Figure 11. Evolution of centroid size (CS) along the phylogeny for the studied species. A, distal partial femur; B, tibia; C, fibula. The cladogram used here is the same composite one as used in Figure 1. Computations were made on log-transformed CS. Values at nodes and along branches were reconstructed based on a Brownian Motion model of evolution (Revell, 2012). Colour codes for taxa follow Figure 1.

strongly correlated with body mass. However, this significant relationship between CS and BM should be considered carefully prior to interpretation, since CS values can be different (or even similar) between taxa depending on the bone considered. This is particularly obvious when comparing *Hyrachyus* and *Teleoceras*, which display similar values of CS for the tibia and the fibula (Fig. 11), whereas the mass of the former taxon was around ten times lower than that of the latter. The relationship between CS and BM is supported by stronger statistical results for the femur, for which size, mass and shape vary in a more congruent way. These results can also be partially related to the fact that CS is computed using the distance of each landmark to the centroid of the object. Consequently, a long and thin object can have a similar CS value to a short and robust one, as it seems to be the case between *Hyrachyus* and *Teleoceras*. The poor correlation between CS and BM for the zeugopodial elements of the hindlimb highlight the limitations of considering CS as a proxy for BM; the stronger relationship between CS and BM for the stylopod is also seen for the forelimb more so than for the hindlimb (see below and Mallet *et al.*, 2021).

Femur: For the femur, a higher size, mass or degree of brachypody is always associated with an increase of the general bone robustness, which is coherent with previous observations on rhinos (Prothero & Sereno, 1982; Mallet *et al.*, 2019; Etienne *et al.*, 2020b). Moreover, the variation of these variables is associated with that of many similar anatomical areas on the femur, although not always with the same intensity.

The femoral head is particularly affected by an increase of size, mass or brachypody, especially for the two latter variables (Figs 4, 5). The shape and orientation of the femoral head change when these parameters increase, becoming more flattened and proximally oriented. This is likely to indicate a reorientation of the limb (and of its rotation axis), being more vertical and placed closer to the parasagittal axis of the animal when size, weight or brachypody increase. This conformation is classically associated with a 'graviportal' body plan (Gregory, 1912; Osborn, 1929) and its presence in giant Paraceratheriidae confirm that their hip joint is oriented more distally with a femur placed close to the parasagittal plane (Prothero, 2013). However, such reorientation is also present in lighter and more brachypodial species like those in Teleoceratina. This highlights the fact that characters classically associated with graviportality, like the reorientation of the femoral head, can be present in taxa displaying different Bauplan layouts (see below).

Along the femoral shaft, high-intensity shape changes are observed at muscle origination points, which is highlighted more clearly in comparisons of shape with body mass and with brachypody (Fig. 5B, C). Such changes are notably observed in Rhinocerotina for the insertion of the m. vastus lateralis (between the greater trochanter convexity and the third trochanter) and on both medial and lateral supracondylar tuberosities, where the m. gastrocnemius and digit flexors insert. These powerful muscles are respectively the main extensors of the zeugopodium and autopodium (Etienne *et al.*, 2021). Differences in bone shape associated with muscle attachments as organisms increase in mass or brachypody are coherent with more powerful muscles ensuring the propulsion and support of a higher absolute weight or of a body with a lower centre of gravity. Moreover, we observed that the bones of a brachypodial species often form shorter lever arms than in dolichopodial species (i.e. an animal having long limbs). Consequently, at equal mass, muscles will need to produce more power to apply higher forces on these shorter lever arms and ensure efficient movements and body support (McGhee & Frank, 1968; Hildebrand, 1974; Fischer & Blickhan, 2006).

On the distal epiphysis, an increase of CS, BM and GI-MT3 is also always associated with more asymmetrical trochlea and condyles. The asymmetry of the distal epiphysis, previously observed on modern rhinos (Mallet *et al.*, 2019), but also in equids (Hermanson & MacFadden, 1996) and bovids (Kappelman, 1988), is likely associated with the need to resist higher constraints exerted near the sagittal plane in taller and heavier quadrupeds. Surprisingly, this asymmetry seems poorly correlated with the thickening of the medial lip of the trochlea, related to body mass increase only (see below).

Tibia: Contrary to what is observed in the femur, shape variation in the tibia is only significantly correlated with the degree of brachypody and the body mass. On this bone, an increase of both body mass and brachypody is associated with an increase of the general robustness, as well as broader epiphyses. The tibial plateau is clearly wider for high values of BM and GI-MT3 (Figs 9A, 10A–B). The same observation can be made for the distal epiphysis, since the contact surface with the astragalus is wider, which is coherent with a mediolateral enlargement of this bone previously observed among heavy Rhinocerotoidea (Etienne *et al.*, 2020b). Similar epiphyseal broadenings have also been observed in heavy bovids (Etienne *et al.*, 2020a). Such proximal and distal broadenings likely confer a better resistance to the knee and ankle joints by ensuring the dissipation of loading forces due to a higher mass on a larger surface area. Moreover, most of the shape changes common to high mass and brachypody are situated distally to the proximal epiphysis and involve

the tibial fossa, the tibia crest and the lateral side of the shaft. These changes seem to be more strongly linked to brachypody than to body mass (Fig. 10). These areas constitute the insertion sites of powerful flexor muscles, respectively the m. tibialis cranialis, a foot flexor, and the mm. biceps femoris, popliteus, semitendinosus and sartorius, all being flexors of the leg (Etienne *et al.*, 2021). Reinforcement of insertions for flexors and extensors are congruent with the higher forces needed to move a heavier body.

Fibula: The shape variation of the fibula is only significantly correlated with the degree of brachypody (and marginally with the centroid size), making it similar to the results observed for the distal part of the femur (see below). However, no clear increase of robustness is related to an increase of brachypody. Morphological changes mainly involve the head and the proximal part of the shaft, where insert flexor and extensor muscles for digits. The distal part, on which the tendons of these muscles run and which is linked to ankle bones by the collateral ligament, is also affected by shape changes (Antoine, 2002; Fisher *et al.*, 2010; Etienne *et al.*, 2021). Variations of the centroid size and degree of brachypody are accompanied by similar shape changes (i.e. larger bones have larger muscle insertion sites), although these two parameters are not significantly correlated. This indicates that similar shape changes may occur in the fibula of taxa showing different body shapes.

Non-congruent shape variation

Although many shape changes of a given bone appear similarly related to variation of size, mass and brachypody, other morphological modifications can be more directly related to one specific parameter. This is notably the case of the fovea capitis on the femoral head, which is only associated with changes in centroid size. This fovea, where the foveal ligament inserts, may be almost absent in some rhino species like the modern black rhinoceros or the giant *Paraceratherium*. The disappearing of the fovea might be interpreted as the absence of this ligament (Crelin, 1988). However, a previous analysis on the elephant hip indicated that this ligament can be present despite the absence of fovea and attached on the distal ridge of the femoral head (Crelin, 1988). This fossa is present in various taxa, independent of their body mass, their locomotor ecology or their habitat: for example, in bovids (Etienne *et al.*, 2020a), in many carnivorans (Jenkins & Camazine, 1977), in porcupines (Yilmaz, 1998) and even in most archosaurs (Tsai & Holliday, 2015). The functional role of the foveal ligament is poorly known, but is hypothesized to limit the abduction of the femur and prevent the dislocation of the hip joint (Crelin, 1988; Barone, 2010b). Consequently, the shape change associated with an increase of centroid size may not be due to the disappearing of this ligament, but to the displacement of its insertion on the femoral head, which could be related to higher constraints due to size or locomotor behaviour to prevent the hip dislocation if the leg deviates too much from the parasagittal plane during locomotion. However, this fovea is also absent or poorly marked in non-related and lighter taxa like *Diceros bicornis* (Linnaeus, 1758) (Guérin, 1980; Antoine, 2002), making it hard to relate its shape and presence or absence to a high body mass only. At the intraspecific level, this fovea can be more or less developed depending on the age of the specimen (Guérin, 1980; Mallet *et al.*, 2019). Consequently, our results do not allow a precise morphofunctional interpretation of the shape changes of this fovea, which remains to be explored more deeply among quadrupeds in relation with body proportions.

On the femur, all three trochanters modify strongly in association with an increase of CS, BM or GI-MT3, but not always in the same way. An increase of mass and brachypody is associated with a lateral development of the greater trochanter convexity, where the m. gluteus menimus inserts, an extensor of the limb (Etienne *et al.*, 2021). Similarly, an increase of the centroid size is mostly associated with changes in the top of the greater trochanter tuberosity, where the m. gluteus medius inserts, considered as the main limb extensor (Etienne *et al.*, 2021). A higher centroid size is associated with a lower tuberosity developed more caudally. The lateral development of the greater trochanter convexity in heavy and brachypodial taxa and the caudal development of the greater trochanter tuberosity lengthen the lever arms laterally and caudally, allowing slower but more powerful extensions and increasing the mechanical advantage of muscles extending the limb (Hildebrand, 1974). The variation of body mass and brachypody is particularly related to the variation of the lesser trochanter, where muscle x inserts the m. iliopsoas, showing a distal displacement for heavier and more brachypodial species. To a lesser extent, the third trochanter, where inserts the m. gluteus maximus, displays the same distal displacement (with shape changes only associated with variation of gracility index). Both trochanters are then facing each other at midshaft in heavy and brachypodial taxa, constituting longer lever arms for muscles which provide gravitational support, a conformation often observed in heavy taxa (Hildebrand, 1974).

On the distal epiphysis of the femur, the asymmetry of the trochlea is associated with a broadening of the medial lip for high body mass only. This medial lip, also called the medial trochlear ridge, is considered as indicative of the presence of a 'passive stay-apparatus'

in various quadrupeds like equids, rhinos or bovids, allowing the animal to endure long periods of standing during feeding or resting times (Hermanson & MacFadden, 1996). The appearance of this feature, which emerged independently in different lineages (Janis *et al.*, 2012), is hypothesized to be related to habitat complexity (Kappelman, 1988) or to body mass (Hermanson & MacFadden, 1996). Although we did not test the hypothesis of a relation with habitat, results on fossil rhinocerotoids tend to support a link between the development of the medial trochlear ridge and a high body mass, as this feature is present in all heavy taxa (in *Metamynodon*, large Paraceratheriidae and all heavy Rhinocerotidae exceeding a ton). This passive 'lock' of the knee joint likely allows heavy rhinos to stand during feeding or resting times without spending too much energy to counteract gravity. Furthermore, a similar pattern has been observed on the forelimb, with the bicipital groove of the humerus being only associated with changes in body mass (Mallet *et al.*, 2021). As the bicipital groove is also likely involved in a passive-stay apparatus for the forelimb (Hermanson & MacFadden, 1992), these particularly congruent results underline that the development of joint lock systems is directly related to an increase of body mass among Rhinocerotoidea.

Differences in stylopodium and zeugopodium shape changes with body proportions

In accordance with the second hypothesis, the comparison of patterns of shape change clearly highlights that the stylopodium and the zeugopodium do not follow the same trends of morphological variations. Whereas the shape variation of the femur is conjointly related to size, mass and gracility index, that of the tibia appears more highly correlated to the degree of brachypody than to body mass. The shape of the fibula appears related to the degree of brachypody only (and only marginally to size). Beyond the general increase of robustness undergone by the bones in heavy species, these strong differences tend to indicate a functional breakdown between the evolution of the stylopodium and zeugopodium among Rhinocerotoidea, both in fore- and hindlimbs (see below). Hallgrímsson *et al.* (2002) and Young & Hallgrímsson (2005) hypothesized an increase in variation of limb elements along the proximodistal axis, especially in quadrupeds, relating this phenomenon to postnatal processes like functional specialization under specific environmental constraints. Our results tend to confirm these observations among Rhinocerotoideaat the evolutionary level, with distal elements of the limb (tibia and fibula) varying more than proximalones (femur). This decoupling might be related to a divergence in the role of these bones, the femur being more involved in flexion and extension movements of both the hip and leg to ensure propulsion, whereas the tibia mainly ensures weight support and provides attachment for the flexor and extensor muscles of the foot (together with the fibula). The weaker correlation of tibial shape with body mass than with the degree of brachypody tends to indicate that the shape of this bone is more related to the distribution of the weight in the body (i.e. position of the centre of gravity, muscles and other organs) than to the absolute body weight of the species. These results appear as partly contradictory to what has been observed in modern rhinos where zeugopodial shape was more directly linked to body mass than that of the stylopodium (Mallet *et al.*, 2019, 2020). However, the five modern species only represent a small sample of the past diversity of Rhinocerotoidea and belong to a subtribe showing an evolutionary trend different from that of the superfamily (see below). This emphasizes that, at the scale of the whole superfamily, the degree of brachypody (and consequently the body mass repartition and the position of the centre of gravity) may be a major driver of the morphological changes of the hindlimb zeugopodium. Conversely, body mass itself may have a more visible impact at a lower taxonomic level (Mallet *et al.*, 2019, 2020). A similar trend differentiating stylopodium and zeugopodium bones has been observed on forelimb elements of the superfamily (see below and Mallet *et al.*, 2021).

Modularity of the femur

Beyond the strict distinction between the stylopodium and zeugopodium, the multiple investigations of the femur based on complete or partial bone analyses reveal that the shape variations of the whole bone, of the proximal and of the distal parts, respectively, do not exhibit the same relationship with size, mass and gracility index. The shape of the proximal part appears significantly correlated with size, mass and gracility index, similar to that of the complete bone, but the species dispersions in the NJ trees, phylomorphospaces and regression plots for these two data sets highlight noteworthy differences. Small taxa like Hyrachyidae, Hyracodontidae, small Elasmotheriinae and Rhinocerotinae *i.s.* share marked morphological affinities with heavy Paraceratheriidae concerning the whole bone, but this is not the case when looking at its proximal part only. This tends to indicate that the proximal part of the femur undergoes shape modification decoupled from that observed on the rest of the bone between these taxa. This pattern of shape variation appears different from that observed on the humerus of Rhinocerotoidea, where the functional signal was similar between the complete bone and its distal epiphysis (see below and Mallet

et al., 2021). The modifications of the femur notably concern the size and the shape of the trochanters, as well as the head orientation. Conversely, the shape variation of the distal part of the femur is more congruent with that of the tibia and fibula than with the whole femur (high correlation with the degree of brachypody, poor correlation with body mass and no correlation with centroid size). All these observations led us to consider that proximal and distal parts of the femur may represent different morphological modules, i.e. anatomical units 'that [are] tightly integrated internally but relatively independent from other such modules' (Klingenberg, 2008). The congruence between the shape variation of the distal femur and the tibia could indicate that the knee joint, with the inclusion of the patella, displays a modular organization. Similarly, the shape of the proximal femur could covary with the pelvic bone, although this covariation has been proven as weak or non-existent in other mammal groups like equids or marsupials (Hanot *et al.*, 2017; Martín-Serra & Benson, 2019). All these questions remain to be addressed among modern and fossil rhinos through relevant modularity tests (Goswami & Polly, 2010; Klingenberg, 2014).

Bone shape and phylogenetic legacy

The differences in shape variation patterns between the stylopodium and the zeugopodium may be related to functional breakdowns between limb segments. In addition, and except for the fibula (see below), shape as well as size, mass and gracility index carry a strong phylogenetic signal (see Results section). The shape variation of the complete femur remains similar among each clade and does not converge with that of other clades. This likely underlines the importance of the evolutionary legacy on the morphological disparity of this bone. Such differences between clades are less clear for its distal part only, as well as for the tibia, for which some taxa show convergences in shape (e.g. *Aphelops*, *Diaceratherium* and *Elasmotherium*). This tends to confirm previous observations among modern rhinos, indicating a stronger phylogenetic signal in the variation of the stylopodium than in that of the zeugopodium (Mallet *et al.*, 2019, 2020). A similar trend has also been observed in the forelimb (see below) (Mallet *et al.*, 2021).

The fibula appears as an exception among these bones, as its shape and centroid size carry almost no phylogenetic signal. Among the superfamily, only the subtribe Teleoceratina display a relative shape homogeneity for the fibula. No clear link between the shape of the fibula and body mass can be seen within the superfamily either. These observations somewhat echo previous results on modern rhinos, which showed a puzzling intraspecific shape variation exceeding the interspecific variation for this bone (Mallet *et al.*, 2019). In addition, the proximal and distal contact surfaces of the fibula are variably fused with those of the tibia among specimens and species; this fusion may potentially be related to evolutionary legacy, to the high body mass of the concerned species, or to the ontogenetic stage of the individual (Antoine, 2002; Polly, 2007). However, the fusion between these two bones can be observed in different taxa, such as *Ceratotherium*, *Menoceras* or *Teleoceras*, without any obvious trend linked to phylogeny or body mass. This fusion can slightly modify the shape of the fibula, notably the interosseous crest and the size and shape of the distal synostosis surface. Moreover, shape data show important differences between the patterns of variation of the tibia and fibula, suggesting some level of independence between these two bones, as previously observed in modern rhinos (Mallet *et al.*, 2020). The fibula therefore stands out from the other bones by the fact that its variation in shape shows no clear structure, regardless of the observation scale within the superfamily.

Beyond these general trends, some groups among the superfamily follow remarkably different tendencies in their shape variation. Giant Paraceratheriidae, despite their extreme size and mass, rarely possess a shape plotting far away from other Rhinocerotoidea in the different morphospaces. In fact, their hindlimb bones show surprising proximities with some Aceratheriini or Rhinocerotini. This underlines that their extreme size and mass are not reflected in extreme shape conformations and, conversely, that taxa with different body mass can share shape similarities. This proximity could be related to the general body plan of these species: Paraceratheriidae are known to retain a 'cursorial' body plan with a relatively high degree of slenderness (Granger & Gregory, 1936; Prothero, 2013) and their limb bones seem more constrained by this general body organization than by constraints due to high body weight support and propulsion.

Conversely, Teleoceratina is another group deviating from the general trend of shape variation common to the whole superfamily. Teleoceratina often constitute extremes of shape variation, particularly the zeugopodial bones of highly brachypodial taxa like *Teleoceras*. This high degree of brachypody is also encountered in phylogenetically distant genera like *Pleuroceros* and *Chilotherium*, leading to marked shape similarities, especially on the zeugopodium. This convergent condition might be related to particular developmental trends among these groups, leading to a shortening of the distal limb. Such a particular condition may be involved in functional roles specific to these groups, such as walking on soft and unstable grounds (Boada-Saña *et al.*, 2007) or even a semi-aquatic ecology, although this hypothesis seems

unlikely given various works (MacFadden, 1998; Mead, 2000; Mihlbachler, 2003; Prothero, 2005; Clementz *et al.*, 2008; Wang & Secord, 2020). Following these authors, larger feet could help to spread the weight of the animal more effectively when moving on soft soil, enhancing the surface area of the pes and preventing it from sinking into mud. In our view, having robust bones should be viewed as an allometric consequence of a shortening of the limb in those species, this shortening being either related to a semi-aquatic lifestyle or/and to an adaptation for grazing. As the precise lifestyle of short-legged rhinos is still debated nowadays, further investigations on these brachypodial taxa should help to clarify the origin and functional roles of this particular condition.

Differences within and between fore- and hindlimb bones

Comparison with data obtained for forelimb bones clearly underlines that the stylopodial elements of the fore- and hindlimbs share similar patterns of shape variation. The morphological changes of both the humerus and femur appear simultaneously correlated with size, mass and gracility index while also carrying a strong phylogenetic signal. Toward high body mass, both the humerus and femur display an increase of general robustness, associated with the development of both epiphyses, the reinforcement of muscular insertions (mainly for extensors and flexors) and their displacement leading to lengthened lever arms. On the other hand, opposite, zeugopodial elements are mainly impacted by the degree of brachypody (at the scale of the whole superfamily), related to the distribution of the mass within the body rather to the absolute mass itself. Furthermore, the shape of the radius and tibia, both of which are involved in supporting the body weight directly, are more related to mass than ulna and fibula shapes. Highly brachypodial taxa display an increase of robustness and a broadening of the epiphyses as well. Some anatomical areas, like the medial and lateral parts of the proximal epiphysis of both the radius and tibia, show a remarkably similar trend of shape variation towards a high degree of brachypody. All these results partially invalidate the fifth hypothesis, as differences in patterns of shape variation are stronger between the stylopodium and zeugopodium than between the fore- and hindlimbs. Similar observations were partially obtained on modern rhinos (Mallet *et al.*, 2019, 2020) and this general trend may indicate that serial homology between fore- and hindlimb elements remain strong (Young & Hallgrímsson, 2005) despite different functional requirements (Henderson, 1999; Regnault *et al.*, 2013; Panagiotopoulou *et al.*, 2019).

However, some differences in functional role do exist between fore- and hindlimbs. Although body mass is correlated with the gracility index (GI-MC3 computed on the third metacarpal) in the forelimb bones (Mallet *et al.*, 2021), this correlation is not significant with GI-MT3. Yet the distribution of these two indices remains extremely similar, possessing the same means and variance (see Supporting Information, Fig. S5). In other words, the variation in gracility index of the hindlimb is decoupled from that of body mass, while these two parameters (gracility index and body mass) are more closely associated for the forelimb. This highlights differences of general organization between fore- and hindlimbs and supports the idea that forelimb bones among Rhinocerotoidea may be more constrained by weight repartition than are the hindlimb ones, in association with their involvement in other functions like ensuring powerful propulsion (Heglund *et al.*, 1982; Alexander, 1985; Dutto *et al.*, 2006; Henderson, 2006; Regnault *et al.*, 2013; Panagiotopoulou *et al.*, 2019) (Fig. 12).

Moreover, the bones constituting the elbow and knee joints might show a modular organization (the modular condition of the tibia remaining to be tested as well). In the forelimb, the trends in shape variation were similar between the complete humerus and its distal part, which displayed similarities with the proximal ulna (such as a significant correlation with CS, BM and GI simultaneously). Conversely, on the hindlimb, the shape variation of the complete femur is only congruent with that of its proximal part, while that of its distal part is more congruent with that of the tibia. Consequently, if morphological modules exist in the elbow and the knee joints of Rhinocerotoidea, they may not be organized in a homologous way, the former involving the entire humerus and the proximal ulna while the latter would involve only the distal femur and the entire tibia. These differences, which will require further testing, may be related to the distinct joint construction between the fore- and hindlimb. Beyond their respective bending in opposite directions, the elbow joint constitutes a strongly constrained hinge restricted to craniocaudal movements only, formed by the humerus, the radius and the ulna together. Conversely, the knee joint allows slight mediolateral rotations in addition to craniocaudal movements (Hildebrand, 1974), although reduced by the passive stay apparatus. Moreover, the knee joint also differs from the elbow in involving a sesamoid bone, the patella, and should be considered as functionally homologous to the shoulder region (Schmidt & Fischer, 2009). This difference of configuration in those two joints may therefore involve differences in shape patterns of the bones constituting them. Only a larger investigation of potential morphological modules and on the construction of these joints could shed light on these questions.

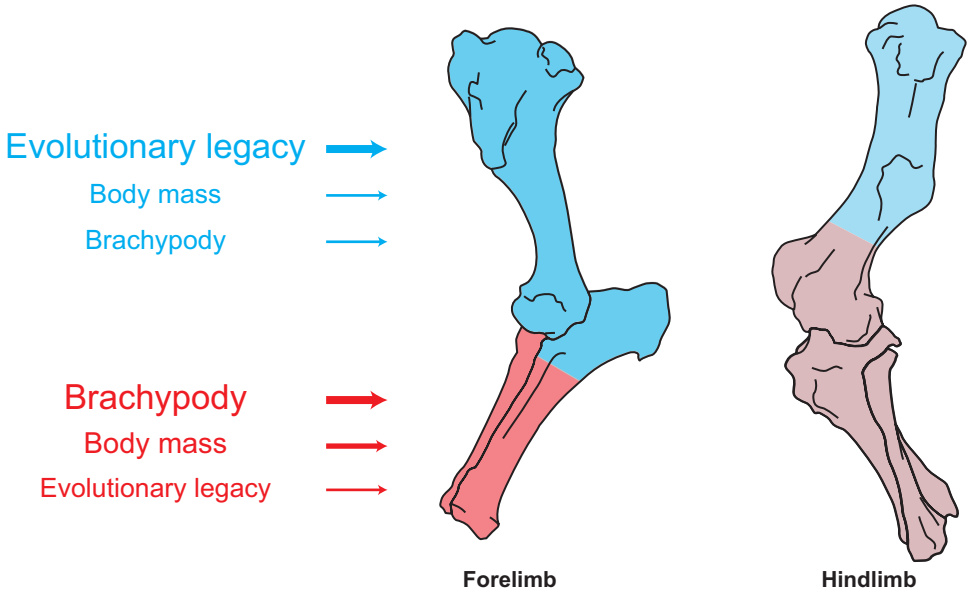

Figure 12. Schematic summary of the relations between bone shape and the different variables tested in this work and in Mallet *et al.* (2021). Blue indicates a shape variation dominated by evolutionary legacy over other parameters. Red indicates a shape variation mainly dominated by brachypody and/or body mass over other parameters. This relative influence is based on the results obtained through the NJ trees, the PCA and the regression plots of the PGLS described in the previous chapters. The size of the font and arrows for each variable is proportional to its relation with the shape for each bone or part of bone based on the overall previous results. Faded colours on the hindlimb indicate a lower association with body mass in general. Bones modified from Archeozoo.org under the Creative Commons license.

GRAVIPORTALITY: AN IRRELEVANT CONCEPT IN RHINOCEROTOIDS?

Finally, the addition of the results on the hindlimb (this study) to those obtained on the forelimb (Mallet *et al.*, 2021) enables the critical evaluation of the concept of graviportality and its application to Rhinocerotoidea (Hutchinson, 2021). The shape of the limb bones in Rhinocerotoidea diversified broadly during the more than 50 Myr of evolution of this group, while its variation still carries a strong phylogenetic signal. Yet, the general construction of the rhino limbs largely follows a similar pattern across the entire superfamily; this 'rhinocerotoid' general pattern being easily distinguishable from those of close relatives (e.g. horses, tapirs) and of other heavy mammals (e.g. proboscideans). Convergences towards a high body mass are observed in other closely related clades within Perissodactyla [e.g. Lophiodontidae and Brontotherioidea exceeding 2000 kg (Damuth & MacFadden, 1990; Robinet *et al.*, 2015) and Chalicotherioidea exceeding 1500 kg (Guérin, 2012)] and in related groups among 'panperissodactyls' (Welker *et al.*, 2015) such as South American native ungulates [Notoungulata and Litopterna sometimes exceeding 1000 kg (MacFadden, 2005; Farina *et al.*, 2014)]. Despite the current lack of interspecific comparative studies of the limb morphology of all these heavy ungulates, they seem to display unique morphologies that share few morphological resemblances with Rhinocerotoidea.

As detailed previously (see Introduction), Gregory (1912) and Osborn (1929) defined graviportal animals by having a relatively long stylopodium and short autopodium, body mass of several hundreds of kilograms, columnar limbs, large and strong bones, large feet and slow pace. When considering this morphofunctional framework and the criteria classically associated with graviportality, no deep architectural breakdown towards this peculiar limb organization has been observed in rhinos. The high body mass and the increase in bone robustness, associated with enlarged feet (although this criterion is relative; Panagiotopoulou *et al.*, 2019), are almost the only graviportal features encountered in the superfamily. The morphology of the elbow and knee joints indicate that almost all taxa in Rhinocerotoidea retain flexed proximal limbs (as in most small and large ungulates in general) with no convergence towards a strictly columnar organization. Only large Paraceratheriidae display straighter limbs, although they are not totally columnar (elbow and knee joints likely remaining flexed, reminiscent of the giraffid sivatheres for example) (Fortelius & Kappelman, 1993; Paul, 1997; Paul & Christiansen, 2000). The lengthening of the stylopodium relative to the other limb elements is

far from being clear except in highly brachypodial species (but more likely due to a shortening of the zeugopodium). The reduction of the autopodium elements (i.e. degree of brachypody) appears associated with various body mass values and not only the highest ones. Conversely, the reduction of the autopodium is not always marked in heavy taxa, as observed in *Elasmotherium* and *Paraceratherium* (Mallet *et al.*, 2021). Although not directly studied here, the gait of rhinos also seems relatively conservative: modern rhinos are able to gallop (Alexander & Pond, 1992) and given the similar general construction of the limbs in large fossil taxa it is likely that most of them could reach a relatively fast pace (Paul & Christiansen, 2000).

Conversely, our detailed study of limb long bones in rhinos highlights the morphological changes undergone by the zeugopodium as rhinocerotoids increased in mass, although this aspect was nearly absent from the classical framework of graviportality. The shape changes observed in the zeugopodial elements relative to the degree of brachypody (and, consequently, to the vertical height of the centre of gravity) shed light on the impact of mass distribution on this segment. While the works of Gregory and Osborn assumed that the relative length of this central segment is poorly modified between cursorial and graviportal taxa (Gregory, 1912; Osborn, 1929), results obtained on rhinocerotoids highlight that, on the contrary, zeugopodium shape is deeply modified between light and heavy rhinos.

Among heavy taxa, Paraceratheriidae challenge the classic definition of graviportality even more than other rhinos (Granger & Gregory, 1936; Fortelius & Kappelman, 1993). In particular, they do not show the relative reduction of the autopodium length or the fully columnar limbs expected for such big quadrupeds. Moreover, the ratio 'humeral length over radial length' is below 1 in *Juxia* and *Urtinotherium* (Paraceratheriidae), but above 1 for the small runner *Hyracodon* (Hyracodontidae), making Paraceratheriidae close to more gracile, specialized cursors such as modern equids (ratio < 1). This ratio is also different from that observed in other rhinos (e.g. > 1 for modern rhinos, C. Mallet, personal computations). Conversely, the ratio 'femoral length over tibial length' is higher in *Paraceratherium* (1.4) than in *Hyrachyus* (1.1) and modern horses (1.1). This ratio on the hindlimb is close to that observed in modern rhinos (1.5 in *Ceratotheriumsimum*, 1.4 in *Diceros Bicornis*) (C. Mallet, personal computations). These ratios, coupled with our results, show that Paraceratheriidae appear to follow a different trend of limb architecture than the rest of the superfamily. Unlike in other Rhinocerotoidea, the shape of their stylopodium is highly derived relative to more basal rhinocerotoids, whereas that of their zeugopodium is poorly modified and retains a plesiomorphic aspect (although relatively more robust) close to that of small taxa like Hyrachyidae and Hyracodontidae (Mallet *et al.*, 2021). This conservative shape of the zeugopodium in paraceratheres is more marked on the forelimb than on the hindlimb, which would appear in contradiction with the forelimb supporting a higher part of the total weight. This atypical pattern of shape variation could be related to the long neck and heavy head borne by paraceratheriids (P.-O. Antoine, pers. comm.), as well as to the slightly sloped backbone (Prothero, 2005), two uncommon features among Rhinocerotoidea which mostly display a short neck and a relatively horizontal spine (Paul & Christiansen, 2000; Qiu & Wang, 2007; Prothero, 2013). It is also possible that the forelimb of Paraceratheriidae does not follow the general trend common to most Rhinocerotoidea, due to strong developmental or evolutionary constraints. All these features highlight morphological features linked to both high body mass support (e.g. robustness of the stylopodium, shortening of the tibia) and the persistence of a cursorial construction close to that of small Hyrachyidae and Hyracodontidae. This unusual architecture tackles the classical opposition between 'cursorial' and 'graviportal' categories, Paraceratheriidae appearing to show features characterizing both categories simultaneously.

Since Rhinocerotoidea hardly display the anatomical criteria classically associated with graviportality, two possible assessments arise: either Rhinocerotoidea should not be considered graviportal, or the graviportal framework is too limited to describe the diverse conditions by which species adapt to heavy weight (Hutchinson, 2021). The limitations of the framework of Gregory (1912) and Osborn (1929) may be related to the archetypal groups used to define graviportality (and cursoriality), as they mainly considered elephants and extinct groups with a similar limb architecture like Dinocerata in this regard (Osborn, 1900). However, it is not certain that all anatomical features originally defined as graviportal in these groups are in fact linked to a high body mass and are shared by all heavy quadrupedal taxa. Most Proboscidea retain poorly modified limbs, with no reduction of the digit number, no radio-ulnar and tibiofibular fusion (however, two traits that are found in Rhinocerotoidea) and a symmetrical femoral trochlea. Their ulna directly supports the humerus in the elbow joint, contrary to the condition in most ungulates, where the humerus is supported almost only by the radius (Fujiwara, 2009; Janis *et al.*, 2012; Larramendi, 2016). Morphofunctional investigations highlight that the limb structure and motion in Proboscidea is atypical compared to that in most mammalian quadrupeds, including heavy ones (Ren *et al.*, 2010). Except in their general increase of robustness, Rhinocerotoidea show

no clear convergence of shape or limb construction with that of Proboscidea, especially in extremely large but gracile taxa like Paraceratheriidae. Most criteria associated with graviportality in elephants are thus not universally shared in heavy quadrupeds showing that the classic graviportal framework should be considered with caution (Hutchinson, 2021). Therefore, it may be more relevant to search for the features repeatedly encountered in diverse taxa showing a high body mass before defining a general concept such as graviportality. As sustaining a heavy weight likely involves a mosaic of traits, the concept of graviportality should only be used after deciphering the repeated features potentially associated with it and the special adaptations limited to each particular group. Taking into account the locomotor behaviour of a given animal should also help to refine the concepts of 'graviportality' and 'cursoriality'.

CONCLUSION

Beyond a common increase of robustness and reinforcement of muscular insertions towards higher body mass, the shape of stylopodial and zeugopodial bones among Rhinocerotoidea does not follow the same pattern of variation. More morphological differences are also observed between the stylopodium and zeugopodium than between fore- and hindlimbs. Rather than the overall absolute body mass, it is the distribution of mass within the body and the resultant position of the centre of gravity (seemingly linked to the degree of brachypody) that seems to drive the shape variation of hindlimb bones. Conversely, only the fibula exhibits a puzzling relationship between shape and body proportions. Our results also highlight the potential modularity of the femur, with a distal region varying in shape in similar ways to the tibia and fibula. Together with our previous results on the forelimb, this points out the need to explore shape patterns beyond the units constituted by single bones. Finally, the integrative investigation of limb bones among Rhinocerotoidea underlines the limits of the concept of graviportality to describe the morphology of these animals. It calls for a refining of this century-old framework, considering the anatomical specificities of each group displaying an increase of body mass through time.

ACKNOWLEDGEMENTS

The authors warmly thank all curators of the visited institutions for granting us access to the studied specimens: E. Hoeger, S. Ketelsen, R. O'Leary and J. Meng (American Museum of Natural History, New York, USA), J.-M. Pouillon and C. Bouix (Association Rhinopolis, Gannat, France), G. Rößner (Bayerische Staatssammlung für Paläontologie und Geologie, Munich, Germany), D. Berthet (Centre de Conservation et d'Étude des Collections, Musée des Confluences, Lyon, France), E. Robert (Collections de Géologie de Lyon, Université Lyon 1 Claude Bernard, Lyon, France), Y. Laurent (Muséum d'Histoire Naturelle de Toulouse, Toulouse, France), J. Lesur and A. Verguin (Muséum National d'Histoire Naturelle, Paris, France), R. Portela-Miguez, P. Brewer and R. Pappa (Natural History Museum, London, UK), L. Costeur and F. Dammeyer (Naturhistorisches Museum Basel, Basel, Switzerland), A. Folie, C. Cousin, O. Pauwels and S. Bruaux (Royal Belgian Institute of Natural Sciences, Brussels, Belgium), E. Gilissen (Royal Museum for Central Africa, Tervuren, Belgium) and D. Brinkman (Yale Peabody Museum, New Haven, CT, USA). We would also like to thank M.C. Reyes from the National Museum of the Philippines (Manila, Philippines) and T. Ingicco from the MNHN (Paris, France) for providing the 3D models of *N. philippinensis*, and J. Hutchinson from the Royal Veterinary College (London, UK) for providing us CT-scan data coming from the University of California Museum of Paleontology (Berkeley, USA). We are grateful to S. Castiglione and P. Raia (University of Naples Federico II, Naples, Italy) for their help in using the RRphylo package. We warmly thank P.-O. Antoine and one anonymous reviewer for their positive and constructive comments allowing us to greatly improve the final quality of this work. Many thanks to K. Gaignebet and C. Bouquet for their help in reconstructing many 3D models. C.M. acknowledges C. Etienne, R. Lefebvre and R. Pintore (MNHN, Paris, France) for constructive discussions and advice on R programming, data analyses and interpretations. The authors declare that there is no conflict of interest.

FUNDING

This work was funded by the European Research Council and is part of the GRAVIBONE project (ERC-2016-STG-715300).

AUTHOR CONTRIBUTIONS

C.M. designed the study with significant inputs from A.H., R.C. and G.B. C.M. carried out the data acquisition with input from A.H. C.M. performed the analyses with the help of R.C and G.B. and all authors interpreted the results. C.M. drafted the manuscript. All authors reviewed and contributed to the final version of the manuscript.

DATA AVAILABILITY

The data underlying this article will be shared on reasonable request to the corresponding author. Most of the 3D models will be or have been deposited on the 3D online repository MorphoSource at the following address: https://www.morphosource.org/projects/000366286?locale=en

REFERENCES

3D Systems Corporation. 2014. *Geomagic Studio*. Rock Hill: 3D Systems Corporation.

Adams DC. 2014. A generalized K statistic for estimating phylogenetic signal from shape and other high-dimensional multivariate data. *Systematic Biology* **63:** 685–697.

Adams DC, **Collyer ML. 2018.** Multivariate phylogenetic comparative methods: evaluations, comparisons, and recommendations. *Systematic Biology* **67:** 14–31.

Adams DC, **Otárola-Castillo E. 2013.** Geomorph: an r package for the collection and analysis of geometric morphometric shape data. *Methods in Ecology and Evolution* **4:** 393–399.

Adams DC, **Rohlf FJ**, **Slice DE. 2004.** Geometric morphometrics: ten years of progress following the 'revolution'. *Italian Journal of Zoology* **71:** 5–16.

Agisoft. 2018. *PhotoScan Professional Edition*. St. Petersburg: Agisoft.

Alexander RM. 1985. Mechanics of posture and gait of some large dinosaurs. *Zoological Journal of the Linnean Society* **83:** 1–25.

Alexander RM, **Pond CM. 1992.** Locomotion and bone strength of the white rhinoceros, *Ceratotherium simum*. *Journal of Zoology* **227:** 63–69.

Antoine PO. 2002. Phylogénie et évolution des Elasmotheriina (Mammalia, Rhinocerotidae). *Mémoires du Muséum National d'Histoire Naturelle* **188:** 5–350.

Antoine PO, **Downing KF**, **Crochet JY**, **Duranthon F**, **Flynn LJ**, **Marivaux L**, **Métais G**, **Rajpar AR**, **Roohi G. 2010.** A revision of *Aceratherium blanfordi* Lydekker, 1884 (Mammalia: Rhinocerotidae) from the Early Miocene of Pakistan: postcranials as a key. *Zoological Journal of the Linnean Society* **160:** 139–194.

Antoine PO, **Duranthon F**, **Welcomme JL. 2003.** *Alicornops* (Mammalia, Rhinocerotidae) dans le Miocène supérieur des Collines Bugti (Balouchistan, Pakistan): implications phylogénétiques. *Geodiversitas* **25:** 575–603.

Antoine PO, **Reyes MC**, **Amano N**, **Bautista AP**, **Chang CH**, **Claude J**, **De Vos J**, **Ingicco T. 2021.** A new rhinoceros clade from the Pleistocene of Asia sheds light on mammal dispersals to the Philippines. *Zoological Journal of the Linnean Society,* **194**(2):416–430. doi:https://doi.org/10.1093/zoolinnean/zlab009.

Arambourg C. 1959. Vertébrés continentaux du Miocène supérieur de l'Afrique du Nord. *Publications du Service de la Carte Géologique de l'Algérie (Nouvelle Série), Paléontologie, Mémoire, Serv. de la Carte Géol. de l'Algérie* **4:** 1–161.

Artec 3D. 2018. *Artec Studio Professional*. Luxembourg: Artec 3D.

Averianov A, **Danilov I**, **Jin J**, **Wang Y. 2017.** A new amynodontid from the Eocene of south China and phylogeny of Amynodontidae (Perissodactyla: Rhinocerotoidea). *Journal of Systematic Palaeontology* **15:** 927–945.

Bai B, **Meng J**, **Wang YQ**, **Wang HB**, **Holbrook L. 2017.** Osteology of the Middle Eocene ceratomorph *Hyrachyus modestus* (Mammalia, Perissodactyla). *Bulletin of the American Museum of Natural History* **413:** 1–70.

Bai B, **Meng J**, **Zhang C**, **Gong YX**, **Wang YQ. 2020.** The origin of Rhinocerotoidea and phylogeny of Ceratomorpha (Mammalia, Perissodactyla). *Communications Biology* **3:** 1–16.

Baker J, **Meade A**, **Pagel M**, **Venditti C. 2015.** Adaptive evolution toward larger size in mammals. *Proceedings of the National Academy of Sciences of the USA* **112:** 5093–5098.

Bardua C, **Felice RN**, **Watanabe A**, **Fabre AC**, **Goswami A. 2019.** A practical guide to sliding and surface semilandmarks in morphometric analyses. *Integrative Organismal Biology* **1:** 1–34.

Barone R. 2010a. *Anatomie comparée des mammifères domestiques. Tome 1: Ostéologie*. Paris: Vigot Frères.

Barone R. 2010b. *Anatomie comparée des mammifères domestiques. Tome 2: Arthrologie et myologie*. Paris: Vigot Frères.

Baylac M, **Frieß M. 2005.** Fourier descriptors, Procrustes superimposition, and data dimensionality: an example of cranial shape analysis in modern human populations. In: Slice DE, ed. *Developments in primatology: progress and prospects. Modern morphometrics in physical anthropology*. Boston: Springer, 145–165.

Becker D. 2003. *Paléoécologie et paléoclimats de la molasse du Jura (Oligo-Miocène)*. Unpublished thesis, Université de Fribourg.

Becker D, **Antoine PO**, **Maridet O. 2013.** A new genus of Rhinocerotidae (Mammalia, Perissodactyla) from the Oligocene of Europe. *Journal of Systematic Palaeontology* **11:** 947–972.

Becker D, **Bürgin T**, **Oberli U**, **Scherler L. 2009.** *Diaceratherium lemanense* (Rhinocerotidae) from Eschenbach (eastern Switzerland): systematics, palaeoecology, palaeobiogeography. *Neues Jahrbuch für Geologie und Paläontologie-Abhandlungen* **254:** 5–39.

Bertram JEA, **Biewener AA. 1990.** Differential scaling of the long bones in the terrestrial carnivora and other mammals. *Journal of Morphology* **204:** 157–169.

Biasatti D, **Wang Y**, **Deng T. 2018.** Paleoecology of Cenozoic rhinos from northwest China: a stable isotope perspective. *Vertebrata PalAsiatica* **56:** 45–68.

Biewener AA. 1989a. Mammalian terrestrial locomotion and size. *BioScience* **39:** 776–783.

Biewener AA. 1989b. Scaling body support in mammals: limb posture and muscle mechanics. *Science* **245:** 45–48.

Biewener AA, **Patek SN. 2018.** *Animal locomotion*. New York: Oxford University Press.

Billet G, **Bardin J. 2021.** Segmental series and size: clade-wide investigation of molar proportions reveals a major

evolutionary allometry in the dentition of placental mammals. *Systematic Biology* **70:** 1101–1109.

Blomberg SP, **Garland T**, **Ives AR**, **Crespi B. 2003.** Testing for phylogenetic signal in comparative data: behavioral traits are more labile. *Evolution* **57:** 717–745.

Boada-Saña A. 2008. *Phylogénie du rhinocérotidé* Diaceratherium *Dietrich, 1931 (Mammalia, Perissodactyla)*. Doctoral dissertation, Bibliothèque cantonale jurassienne.

Boada-Saña A, **Hervet S**, **Antoine PO. 2007.** Nouvelles données sur les rhinocéros fossiles de Gannat (Allier, limite Oligocène-Miocène). *Revue des Sciences Naturelles d'Auvergne* **71:** 3–25.

Bokma F, **Godinot M**, **Maridet O**, **Ladevèze S**, **Costeur L**, **Solé F**, **Gheerbrant E**, **Peigné S**, **Jacques F**, **Laurin M. 2016.** Testing for Depéret's rule (body size increase) in mammals using combined extinct and extant data. *Systematic Biology* **65:** 98–108.

Botton-Divet L, **Cornette R**, **Fabre AC**, **Herrel A**, **Houssaye A. 2016.** Morphological analysis of long bones in semi-aquatic mustelids and their terrestrial relatives. *Integrative and Comparative Biology* **56:** 1298–1309.

Botton-Divet L, **Cornette R**, **Houssaye A**, **Fabre AC**, **Herrel A. 2017.** Swimming and running: a study of the convergence in long bone morphology among semi-aquatic mustelids (Carnivora: Mustelidae). *Biological Journal of the Linnean Society* **121:** 38–49.

Cappellini E, **Welker F**, **Pandolfi L**, **Ramos-Madrigal J**, **Samodova D**, **Rüther PL**, **Fotakis AK**, **Lyon D**, **Moreno-Mayar JV**, **Bukhsianidze M**, **Jersie-Christensen RR**, **Mackie M**, **Ginolhac A**, **Ferring R**, **Tappen M**, **Palkopoulou E**, **Dickinson MR**, **Stafford TW**, **Chan YL**, **Götherström A**, **Nathan SKSS**, **Heintzman PD**, **Kapp JD**, **Kirillova I**, **Moodley Y**, **Agusti J**, **Kahlke RD**, **Kiladze G**, **Martínez-Navarro B**, **Liu S**, **Velasco MS**, **Sinding MHS**, **Kelstrup CD**, **Allentoft ME**, **Orlando L**, **Penkman K**, **Shapiro B**, **Rook L**, **Dalén L**, **Gilbert MTP**, **Olsen JV**, **Lordkipanidze D**, **Willerslev E. 2019.** Early Pleistocene enamel proteome from Dmanisi resolves *Stephanorhinus* phylogeny. *Nature* **574:** 103–107.

Carrano MT. 1999. What, if anything, is a cursor? Categories versus continua for determining locomotor habit in mammals and dinosaurs. *Journal of Zoology* **247:** 29–42.

Cassini GH, **Vizcaíno SF**, **Bargo MS. 2012.** Body mass estimation in Early Miocene native South American ungulates: a predictive equation based on 3D landmarks. *Journal of Zoology* **287:** 53–64.

Castiglione S, **Tesone G**, **Piccolo M**, **Melchionna M**, **Mondanaro A**, **Serio C**, **Febbraro MD**, **Raia P. 2018.** A new method for testing evolutionary rate variation and shifts in phenotypic evolution. *Methods in Ecology and Evolution* **9:** 974–983.

Cerdeño E. 1995. Cladistic analysis of the family Rhinocerotidae (Perissodactyla). *American Museum Novitates* **3143:** 1–25.

Cerdeño E. 1998. Diversity and evolutionary trends of the Family Rhinocerotidae (Perissodactyla). *Palaeogeography, Palaeoclimatology, Palaeoecology* **141:** 13–34.

Chen S, **Deng T**, **Hou S**, **Shi Q**, **Pang L. 2010.** Sexual dimorphism in perissodactyl rhinocerotid *Chilotherium wimani* from the Late Miocene of the Linxia Basin (Gansu, China). *Acta Palaeontologica Polonica* **55:** 587–597.

Cignoni P, **Callieri M**, **Corsini M**, **Dellepiane M**, **Ganovelli F**, **Ranzuglia G. 2008.** *MeshLab: an open-source mesh processing tool*. Geneva: Eurographics European Association for Computer Graphics.

Clementz MT, **Holroyd PA**, **Koch PL. 2008.** Identifying aquatic habits of herbivorous mammals through stable isotope analysis. *Palaios* **23:** 574–585.

Colbert EH. 1938. Fossil mammals from Burma in the American Museum of Natural History. *Bulletin of the American Museum of Natural History* **74:** 255–436.

Coombs WP. 1978. Theoretical aspects of cursorial adaptations in dinosaurs. *Quarterly Review of Biology* **53:** 393–418.

Cope ED. 1887. *The origin of the fittest: essays on evolution*. New York: Appleton.

Crelin ES. 1988. Ligament of the head of the femur in the orangutan and Indian elephant. *Yale Journal of Biology and Medicine* **61:** 383–388.

Damuth JD, **MacFadden BJ. 1990.** *Body size in mammalian paleobiology: estimation and biological implications*. Cambridge: Cambridge University Press.

Depéret C. 1907. *Les transformations du monde animal*. Paris: Flammarion.

Dinerstein E. 1991. Sexual dimorphism in the greater one-horned rhinoceros (*Rhinoceros unicornis*). *Journal of Mammalogy* **72:** 450–457.

Dinerstein E. 2011. Family Rhinocerotidae (Rhinoceroses). In: Wilson DE, Mittermeier RA, eds. *Handbook of the mammals of the world*. Barcelona: Lynx Edicions, 144–181.

Dutto DJ, **Hoyt DF**, **Clayton HM**, **Cogger EA**, **Wickler SJ. 2006.** Joint work and power for both the forelimb and hindlimb during trotting in the horse. *Journal of Experimental Biology* **209:** 3990–3999.

Eisenmann V, **Guérin C. 1984.** Morphologie fonctionnelle et environnement chez les périssodactyles. *Geobios* **17:** 69–74.

Ercoli MD, **Prevosti FJ. 2011.** Estimación de masa de las especies de Sparassodonta (Mammalia, Metatheria) de edad Santacrucense (Mioceno Temprano) a partir del tamaño del centroide de los elementos apendiculares: inferencias paleoecológicas. *Ameghiniana* **48:** 462–479.

Etienne C, **Filippo A**, **Cornette R**, **Houssaye A. 2020a.** Effect of mass and habitat on the shape of limb long bones: a morpho-functional investigation on Bovidae (Mammalia: Cetartiodactyla). *Journal of Anatomy* **238:** 886–904.

Etienne C, **Houssaye A**, **Hutchinson JR. 2021.** Limb myology and muscle architecture of the Indian rhinoceros *Rhinoceros unicornis* and the white rhinoceros *Ceratotherium simum* (Mammalia: Rhinocerotidae). *PeerJ* **9:** e11314.

Etienne C, **Mallet C**, **Cornette R**, **Houssaye A. 2020b.** Influence of mass on tarsus shape variation: a morphometrical investigation among Rhinocerotidae (Mammalia: Perissodactyla). *Biological Journal of the Linnean Society* **129:** 950–974.

Farina RA, **Czerwonogora A**, **Giacomo MD. 2014.** Splendid oddness: revisiting the curious trophic relationships of South American Pleistocene mammals and their abundance. *Anais da Academia Brasileira de Ciências* **86:** 311–331.

Fau M, **Cornette R**, **Houssaye A. 2016.** Photogrammetry for 3D digitizing bones of mounted skeletons: potential and limits. *Comptes Rendus Palevol* **15:** 968–977.

Federative Committee on Anatomical Terminology. **1998.** *Terminologia anatomica*. Leipzig, New York: Georg Thieme Verlag.

Felsenstein J. 1985. Phylogenies and the comparative method. *The American Naturalist* **125:** 1–15.

Felsenstein J. 2004. *Inferring phylogenies*. Sunderland: Oxford University Press.

Fernando P, **Polet G**, **Foead N**, **Ng LS**, **Pastorini J**, **Melnick DJ. 2006.** Genetic diversity, phylogeny and conservation of the Javan rhinoceros (*Rhinoceros sondaicus*). *Conservation Genetics* **7:** 439–448.

Fischer MS, **Blickhan R. 2006.** The tri-segmented limbs of therian mammals: kinematics, dynamics, and self-stabilization—a review. *Journal of Experimental Zoology Part A: Comparative Experimental Biology* **305A:** 935–952.

Fisher RE, **Scott KM**, **Adrian B. 2010.** Hind limb myology of the common hippopotamus, *Hippopotamus amphibius* (Artiodactyla: Hippopotamidae). *Zoological Journal of the Linnean Society* **158:** 661–682.

Fortelius M, **Kappelman J. 1993.** The largest land mammal ever imagined. *Zoological Journal of the Linnean Society* **108:** 85–101.

Fujiwara S. 2009. Olecranon orientation as an indicator of elbow joint angle in the stance phase, and estimation of forelimb posture in extinct quadruped animals. *Journal of Morphology* **270:** 1107–1121.

Gaudry M. 2017. *Molecular phylogenetics of the rhinoceros clade and evolution of UCP1 transcriptional regulatory elements across the mammalian phylogeny*. Unpublished thesis, University of Manitoba. Available at: https://mspace.lib.umanitoba.ca/handle/1993/32525.

Goolsby EW. 2015. Phylogenetic comparative methods for evaluating the evolutionary history of function-valued traits. *Systematic Biology* **64:** 568–578.

Goswami A, **Polly PD. 2010.** Methods for studying morphological integration and modularity. *The Paleontological Society Papers* **16:** 213–243.

Gower JC. 1975. Generalized Procrustes analysis. *Psychometrika* **40:** 33–51.

Granger W, **Gregory WK. 1936.** Further notes on the gigantic extinct rhinoceros, *Baluchitherium*, from the Oligocene of Mongolia. *Bulletin of the American Museum of Natural History* **72:** 1–73.

Gregory WK. 1912. Notes on the principles of quadrupedal locomotion and on the mechanism of the limbs in hoofed animals. *Annals of the New York Academy of Sciences* **22:** 267–294.

Guérin C. 1980. Les Rhinocéros (Mammalia, Perissodactyla) du Miocène terminal au Pléistocène supérieur en Europe occidentale. Comparaison avec les espèces actuelles. *Travaux et Documents des Laboratoires de Géologie de Lyon* **79:** 3–421.

Guérin C. 1989. La famille des Rhinocerotidae (Mammalia, Perissodactyla): systématique, histoire, évolution, paléoécologie. *Cranium* **6:** 3–14.

Guérin C. 2012. *Anisodon grande* (Perissodactyla, Chalicotheriidae) de Sansan. *Mémoires du Muséum National d'Histoire Naturelle* **203:** 279–315.

Gunz P, **Mitteroecker P. 2013.** Semilandmarks: a method for quantifying curves and surfaces. *Hystrix* **24:** 103–109.

Gunz P, **Mitteroecker P**, **Bookstein FL. 2005.** Semilandmarks in three dimensions. In: Slice DE, ed. *Developments in primatology: progress and prospects. Modern morphometrics in physical anthropology*. Boston: Springer, 73–98.

Hallgrímsson B, **Katz DC**, **Aponte JD**, **Larson JR**, **Devine J**, **Gonzalez PN**, **Young NM**, **Roseman CC**, **Marcucio RS. 2019.** Integration and the developmental genetics of allometry. *Integrative and Comparative Biology* **59:** 1369–1381.

Hallgrímsson B, **Willmore K**, **Hall BK. 2002.** Canalization, developmental stability, and morphological integration in primate limbs. *American Journal of Physical Anthropology* **119:** 131–158.

Hanot P, **Herrel A**, **Guintard C**, **Cornette R. 2017.** Morphological integration in the appendicular skeleton of two domestic taxa: the horse and donkey. *Proceedings of the Royal Society series B* **284:** 20171241.

Heglund NC, **Cavagna GA**, **Taylor CR. 1982.** Energetics and mechanics of terrestrial locomotion. III. Energy changes of the centre of mass as a function of speed and body size in birds and mammals. *Journal of Experimental Biology* **97:** 41–56.

Heissig K. 2012. Les Rhinocerotidae (Perissodactyla) de Sansan. *Mémoires du Muséum National d'Histoire Naturelle* **203:** 317–485.

Henderson DM. 1999. Estimating the masses and centers of mass of extinct animals by 3-D mathematical slicing. *Paleobiology* **25:** 88–106.

Henderson DM. 2006. Burly gaits: centers of mass, stability, and the trackways of sauropod dinosaurs. *Journal of Vertebrate Paleontology* **26:** 907–921.

Hermanson JW, **MacFadden BJ. 1992.** Evolutionary and functional morphology of the shoulder region and stay-apparatus in fossil and extant horses (Equidae). *Journal of Vertebrate Paleontology* **12:** 377–386.

Hermanson JW, **MacFadden BJ. 1996.** Evolutionary and functional morphology of the knee in fossil and extant horses (Equidae). *Journal of Vertebrate Paleontology* **16:** 349–357.

Hildebrand M. 1974. *Analysis of vertebrate structure*. New York: John Wiley & Sons.

Ho J, **Tumkaya T**, **Aryal S**, **Choi H**, **Claridge-Chang A. 2019.** Moving beyond P values: data analysis with estimation graphics. *Nature Methods* **16:** 565–566.

Houssaye A, **Fernandez V**, **Billet G. 2016.** Hyperspecialization in some South American endemic ungulates revealed by long bone microstructure. *Journal of Mammalian Evolution* **23:** 221–235.

Hullot M, **Antoine PO. 2020.** Mortality curves and population structures of Late Early Miocene Rhinocerotidae (Mammalia, Perissodactyla) remains from the Béon 1 locality of Montréal-du-Gers, France. *Palaeogeography, Palaeoclimatology, Palaeoecology* **558:** 109938.

Hutchinson JR. 2021. The evolutionary biomechanics of locomotor function in giant land animals. *Journal of Experimental Biology* **224:** jeb217463.

Ives AR. 2019. R^2s for correlated data: phylogenetic models, LMMs, and GLMMs. *Systematic Biology* **68:** 234–251.

Janis CM, **Shoshitaishvili B**, **Kambic R**, **Figueirido B. 2012.** On their knees: distal femur asymmetry in ungulates and its relationship to body size and locomotion. *Journal of Vertebrate Paleontology* **32:** 433–445.

Jenkins FA, **Camazine SM. 1977.** Hip structure and locomotion in ambulatory and cursorial carnivores. *Journal of Zoology* **181:** 351–370.

Kappelman J. 1988. Morphology and locomotor adaptations of the bovid femur in relation to habitat. *Journal of Morphology* **198:** 119–130.

Klingenberg CP. 2008. Morphological integration and developmental modularity. *Annual Review of Ecology, Evolution, and Systematics* **39:** 115–132.

Klingenberg CP. 2014. Studying morphological integration and modularity at multiple levels: concepts and analysis. *Philosophical Transactions of the Royal Society B: Biological Sciences* **369:** 20130249.

Klingenberg CP. 2016. Size, shape, and form: concepts of allometry in geometric morphometrics. *Development Genes and Evolution* **226:** 113–137.

Klingenberg CP, **Marugán-Lobón J. 2013.** Evolutionary covariation in geometric morphometric data: analyzing integration, modularity, and allometry in a phylogenetic context. *Systematic Biology* **62:** 591–610.

Larramendi A. 2016. Shoulder height, body mass and shape of proboscideans. *Acta Palaeontologica Polonica* **61:** 537–574.

Lessertisseur J, **Saban R. 1967.** Le squelette. Squelette appendiculaire. In: Grassé P-P, ed. *Traité de zoologie. Tome XVI, fascicule 1: mammifères*. Paris: Masson, 298–1123.

Liu S, **Westbury MV**, **Dussex N**, **Mitchell KJ**, **Sinding MHS**, **Heintzman PD**, **Duchêne DA**, **Kapp JD**, **von Seth J**, **Heiniger H**, **Sánchez-Barreiro F**, **Margaryan A**, **André-Olsen R**, **Cahsan BD**, **Meng G**, **Yang C**, **Chen L**, **van der Valk T**, **Moodley Y**, **Rookmaaker K**, **Bruford MW**, **Ryder O**, **Steiner C**, **Bruins-van Sonsbeek LGR**, **Vartanyan S**, **Guo C**, **Cooper A**, **Kosintsev P**, **Kirillova I**, **Lister AM**, **Marques-Bonet T**, **Gopalakrishnan S**, **Dunn RR**, **Lorenzen ED**, **Shapiro B**, **Zhang G**, **Antoine PO**, **Dalén L**, **Gilbert MTP. 2021.** Ancient and modern genomes unravel the evolutionary history of the rhinoceros family. *Cell* **184:** 4874–4885.

Lu X. 2013. A juvenile skull of *Acerorhinus yuanmouensis* (Mammalia: Rhinocerotidae) from the Late Miocene hominoid fauna of the Yuanmou Basin (Yunnan, China). *Geobios* **46:** 539–548.

MacFadden BJ. 1998. Tale of two rhinos: isotopic ecology, paleodiet, and niche differentiation of *Aphelops* and *Teloceras* from the Florida Neogene. *Paleobiology* **24:** 274–286.

MacFadden BJ. 2005. Diet and habitat of toxodont megaherbivores (Mammalia, Notoungulata) from the Late Quaternary of South and Central America. *Quaternary Research* **64:** 113–124.

Maddison WP, **Maddison DR. 2021.** *Mesquite: a modular system for evolutionary analysis*. Available at: https://www.mesquiteproject.org

Mallet C, **Billet G**, **Houssaye A**, **Cornette R. 2020.** A first glimpse at the influence of body mass in the morphological integration of the limb long bones: an investigation in modern rhinoceroses. *Journal of Anatomy* **237:** 704–726.

Mallet C, **Cornette R**, **Billet G**, **Houssaye A. 2019.** Interspecific variation in the limb long bones among modern rhinoceroses—extent and drivers. *PeerJ* **7:** e7647.

Mallet C, **Houssaye A**, **Cornette R**, **Billet G. 2021.** Long bone shape variation in the forelimb of Rhinocerotoidea: relation with size, body mass and body proportions. *Zoological Journal of the Linnean Society,* zlab095. 1–34. doi:https://doi.org/10.1093/zoolinnean/zlab095.

Mallison H, **Wings O. 2014.** Photogrammetry in paleontology - a practical guide. *Journal of Paleontological Techniques* **12:** 1–31.

Martins EP, **Hansen TF. 1997.** Phylogenies and the comparative method: a general approach to incorporating phylogenetic information into the analysis of interspecific data. *The American Naturalist* **149:** 646–667.

Martín-Serra A, **Benson RBJ. 2019.** Developmental constraints do not influence long-term phenotypic evolution of marsupial forelimbs as revealed by interspecific disparity and integration patterns. *The American Naturalist* **195:** 547–560.

McGhee RB, **Frank AA. 1968.** On the stability properties of quadruped creeping gaits. *Mathematical Biosciences* **3:** 331–351.

Mead AJ. 2000. Sexual dimorphism and paleoecology in *Teleoceras*, a North American Miocene rhinoceros. *Paleobiology* **26:** 689–706.

Mihlbachler MC. 2003. Demography of Late Miocene rhinoceroses (*Teleoceras proterum* and *Aphelops malacorhinus*) from Florida: linking mortality and sociality in fossil assemblages. *Paleobiology* **29:** 412–428.

Mihlbachler MC. 2007. Sexual dimorphism and mortality bias in a small Miocene North American rhino, *Menoceras arikarense*: insights into the coevolution of sexual dimorphism and sociality in rhinos. *Journal of Mammalian Evolution* **14:** 217–238.

Mitteroecker P, **Gunz P**, **Windhager S**, **Schaefer K. 2013.** A brief review of shape, form, and allometry in geometric morphometrics, with applications to human facial morphology. *Hystrix* **24:** 59–66.

Orlando L, **Leonard JA**, **Thenot A**, **Laudet V**, **Guerin C**, **Hänni C. 2003.** Ancient DNA analysis reveals woolly rhino evolutionary relationships. *Molecular Phylogenetics and Evolution* **28:** 485–499.

Osborn HF. 1900. The angulation of the limbs of Proboscidia, Dinocerata, and other quadrupeds, in adaptation to weight. *The American Naturalist* **34:** 89–94.

Osborn HF. 1929. *The titanotheres of ancient Wyoming, Dakota, and Nebraska*. Washington, DC: Government Printing Office.

Panagiotopoulou O, **Pataky TC**, **Hutchinson JR. 2019.** Foot pressure distribution in white rhinoceroses (*Ceratotherium simum*) during walking. *PeerJ* **7:** e6881.

Paradis E, **Schliep K. 2019.** ape 5.0: an environment for modern phylogenetics and evolutionary analyses in R. *Bioinformatics* **35:** 526-528.

Paul GS. 1997. Dinosaur models: the good, the bad, and using them to estimate the mass of dinosaurs. In: Wolberg DL, Stump E, Rosenberg G, eds. *Dinofest International: proceedings of a symposium held at Arizona State University*. Philadelphia: The Academy of Natural Sciences, 129–154.

Paul GS, **Christiansen P. 2000.** Forelimb posture in neoceratopsian dinosaurs: implications for gait and locomotion. *Paleobiology* **26:** 450–465.

Piras P, **Maiorino L**, **Raia P**, **Marcolini F**, **Salvi D**, **Vignoli L**, **Kotsakis T. 2010.** Functional and phylogenetic constraints in Rhinocerotinae craniodental morphology. *Evolutionary Ecology Research* **12:** 897–928.

Polly PD. 2007. Limbs in mammalian evolution. Chapter 15. In: Hall BK, ed. *Fins into limbs: evolution, development, and transformation*. Chicago: University of Chicago Press, 245–268.

Price SA, **Bininda-Emonds ORP. 2009.** A comprehensive phylogeny of extant horses, rhinos and tapirs (Perissodactyla) through data combination. *Zoosystematics and Evolution* **85:** 277–292.

Prothero DR. 1998. Hyracodontidae. In: Janis CM, Scott KM, Jacobs LL, eds. *Evolution of Tertiary mammals of North America: volume 1, terrestrial carnivores, ungulates, and ungulate like mammals*. Cambridge: Cambridge University Press, 589–593.

Prothero DR. 2005. *The evolution of North American rhinoceroses*. Cambridge: Cambridge University Press.

Prothero DR. 2013. *Rhinoceros giants: the paleobiology of Indricotheres*. Bloomington: Indiana University Press.

Prothero DR, **Schoch RM. 1989.** *The evolution of perissodactyls*. New York: Oxford University Press.

Prothero DR, **Sereno PC. 1982.** Allometry and paleoecology of medial Miocene dwarf rhinoceroses from the Texas Gulf coastal plain. *Paleobiology* **8:** 16–30.

Qiu ZX, **Wang BY. 2007.** Paracerathere fossils of China. *Palaeontologia Sinica, new series C* **29:** 1–396.

R Core Team. **2014.** *R: a language and environment for statistical computing*. Vienna: R Foundation for Statistical Computing.

Raia P, **Carotenuto F**, **Passaro F**, **Fulgione D**, **Fortelius M. 2012.** Ecological specialization in fossil mammals explains Cope's rule. *The American Naturalist* **179:** 328–337.

Regnault S, **Hermes R**, **Hildebrandt T**, **Hutchinson J**, **Weller R. 2013.** Osteopathology in the feet of rhinoceroses: lesion type and distribution. *Journal of Zoo and Wildlife Medicine* **44:** 918–927.

Ren L, **Miller CE**, **Lair R**, **Hutchinson JR. 2010.** Integration of biomechanical compliance, leverage, and power in elephant limbs. *Proceedings of the National Academy of Sciences of the USA* **107:** 7078–7082.

Revell LJ. 2012. Phytools: an R package for phylogenetic comparative biology (and other things). *Methods in Ecology and Evolution* **3:** 217–223.

Robinet C, **Remy JA**, **Laurent Y**, **Danilo L**, **Lihoreau F. 2015.** A new genus of Lophiodontidae (Perissodactyla, Mammalia) from the Early Eocene of La Borie (southern France) and the origin of the genus *Lophiodon* Cuvier, 1822. *Geobios* **48:** 25–38.

Rohlf FJ. 2001. Comparative methods for the analysis of continuous variables: geometric interpretations. *Evolution* **55:** 2143–2160.

Rohlf FJ, **Slice D. 1990.** Extensions of the Procrustes method for the optimal superimposition of landmarks. *Systematic Biology* **39:** 40–59.

Scherler L, **Mennecart B**, **Hiard F**, **Becker D. 2013.** Evolutionary history of hoofed mammals during the Oligocene-Miocene transition in western Europe. *Swiss Journal of Geosciences* **106:** 349–369.

Schlager S. 2017. Chapter 9 - Morpho and Rvcg – Shape analysis in R: R-packages for geometric morphometrics, shape analysis and surface manipulations. In: Zheng G, Li S, Székely G, eds. *Statistical shape and deformation analysis*. London: Academic Press, 217–256.

Schliep KP. 2011. Phangorn: phylogenetic analysis in R. *Bioinformatics* **27:** 592–593.

Schmidt M, **Fischer MS. 2009.** Morphological integration in mammalian limb proportions: dissociation between function and development. *Evolution* **63:** 749–766.

Serio C, **Raia P**, **Meloro C. 2020.** Locomotory adaptations in 3D humerus geometry of Xenarthra: testing for convergence. *Frontiers in Ecology and Evolution* **8:** 139.

Steiner CC, **Ryder OA. 2011.** Molecular phylogeny and evolution of the Perissodactyla. *Zoological Journal of the Linnean Society* **163:** 1289–1303.

Stilson KT, **Hopkins SSB**, **Davis EB. 2016.** Osteopathology in Rhinocerotidae from 50 million years to the present. *PLoS One* **11:** e0146221.

Swenson N. 2014. *Functional and phylogenetic ecology in R*. New York: Springer-Verlag.

Thermo Fisher Scientific. **2018.** *Thermo Scientific Avizo software 9 user's guide*. Berlin: Konrad-Zuse-Zentrum fu¨r Informationstechnik. Available at: https://assets.thermofisher.com/TFS-Assets/MSD/Product-Guides/user-guide-avizo-software.pdf

Tissier J, **Antoine PO**, **Becker D. 2020.** New material of *Epiaceratherium* and a new species of *Mesaceratherium* clear up the phylogeny of early Rhinocerotidae (Perissodactyla). *Royal Society Open Science* **7:** 200633.

Tissier J, **Becker D**, **Codrea V**, **Costeur L**, **Fărcaş C**, **Solomon A**, **Venczel M**, **Maridet O. 2018.** New data on Amynodontidae (Mammalia, Perissodactyla) from eastern Europe: phylogenetic and palaeobiogeographic implications around the Eocene-Oligocene transition. *PLoS One* **13:** e0193774.

Tougard C, **Delefosse T**, **Hänni C**, **Montgelard C. 2001.** Phylogenetic relationships of the five extant rhinoceros species (Rhinocerotidae, Perissodactyla) based on mitochondrial cytochrome b and 12S rRNA genes. *Molecular Phylogenetics and Evolution* **19:** 34–44.

Tsai HP, **Holliday CM. 2015.** Articular soft tissue anatomy of the archosaur hip joint: structural homology and functional implications. *Journal of Morphology* **276:** 601–630.

Wang H, **Bai B**, **Meng J**, **Wang Y. 2016.** Earliest known unequivocal rhinocerotoid sheds new light on the origin of giant rhinos and phylogeny of early rhinocerotoids. *Scientific Reports* **6:** 1–9.

Wang B, **Secord R. 2020.** Paleoecology of *Aphelops* and *Teleoceras* (Rhinocerotidae) through an interval of changing climate and vegetation in the Neogene of the Great Plains, central United States. *Palaeogeography, Palaeoclimatology, Palaeoecology* **542:** 109411.

Wasserstein RL, **Schirm AL**, **Lazar NA. 2019.** Moving to a world beyond 'P < 0.05'. *The American Statistician* **73:** 1–19.

Welker F, **Collins MJ**, **Thomas JA**, **Wadsley M**, **Brace S**, **Cappellini E**, **Turvey ST**, **Reguero M**, **Gelfo JN**, **Kramarz A**, **Burger J**, **Thomas-Oates J**, **Ashford DA**, **Ashton PD**, **Rowsell K**, **Porter DM**, **Kessler B**, **Fischer R**, **Baessmann C**, **Kaspar S**, **Olsen JV**, **Kiley P**, **Elliott JA**, **Kelstrup CD**, **Mullin V**, **Hofreiter M**, **Willerslev E**, **Hublin JJ**, **Orlando L**, **Barnes I**, **MacPhee RDE. 2015.** Ancient proteins resolve the evolutionary history of Darwin's South American ungulates. *Nature* **522:** 81–84.

Welker F, **Smith GM**, **Hutson JM**, **Kindler L**, **Garcia-Moreno A**, **Villaluenga A**, **Turner E**, **Gaudzinski-Windheuser S. 2017.** Middle Pleistocene protein sequences from the rhinoceros genus *Stephanorhinus* and the phylogeny of extant and extinct Middle/Late Pleistocene Rhinocerotidae. *PeerJ* **5:** e3033.

Wiley DF, **Amenta N**, **Alcantara DA**, **Ghosh D**, **Kil YJ**, **Delson E**, **Harcourt-Smith W**, **Rohlf FJ**, **St. John K**, **Hamann B. 2005.** Evolutionary morphing. In: *Proceedings of IEEE Visualization 2005*. Minneapolis, Minnesota: IEEE (Institute of Electrical and Electronic Engineers). Available at: https://ieeexplore.ieee.org/abstract/document/1532826

Willerslev E, **Gilbert MTP**, **Binladen J**, **Ho SY**, **Campos PF**, **Ratan A**, **Tomsho LP**, **da Fonseca RR**, **Sher A**, **Kuznetsova TV**, **Nowak-Kemp M**, **Roth TL**, **Miller W**, **Schuster SC. 2009.** Analysis of complete mitochondrial genomes from extinct and extant rhinoceroses reveals lack of phylogenetic resolution. *BMC Evolutionary Biology* **9:** 951–911.

Yilmaz S. 1998. Macro-anatomical investigations on the skeletons of porcupine (*Hystrix cristata*). Part III: skeleton axiale. *Anatomia, Histologia, Embryologia* **27:** 293–296.

Young NM, **Hallgrímsson B. 2005.** Serial homology and the evolution of mammalian limb covariation structure. *Evolution* **59:** 2691–2704.

Yuan J, **Sheng G**, **Hou X**, **Shuang X**, **Yi J**, **Yang H**, **Lai X. 2014.** Ancient DNA sequences from *Coelodonta antiquitatis* in China reveal its divergence and phylogeny. *Science China Earth Sciences* **57:** 388–396.

Zelditch ML, **Swiderski DL**, **Sheets HD**, **Fink WL. 2012.** *Geometric morphometrics for biologists: a primer*. London: Academic Press.

Zschokke S, **Baur B. 2002.** Inbreeding, outbreeding, infant growth, and size dimorphism in captive Indian rhinoceros (*Rhinoceros unicornis*). *Canadian Journal of Zoology* **80:** 2014–2023.

SUPPORTING INFORMATION

Additional Supporting Information may be found in the online version of this article at the publisher's web-site:

Data S1. Designation and location of the anatomical landmarks placed on each bone.

Figure S1. Summary of the anatomical areas of the rhino long bone. Bones figured here belong to *C. simum*. A, humerus. Abbreviations: F.c.: Fovea capitis; G.t.: Greater trochanter; G.t.c.: Greater trochanter convexity; G.t.t.: Greater trochanter top; H.: Head; I.s.: Intercondylar space; L.c.: Lateral condyle; L.e.: Lateral epicondyle; L.t.r.: Lateral trochlear ridge; L.t.: Lesser trochanter; M.c.: Medial condyle; M.e.: Medial epicondyle; M.t.r.: Medial trochlear ridge; N.: Neck; S.f.: Supracondylar fossa; T.: Trochlea; T.f.: Trochanteric fossa; T.g.: Trochlear groove; T.t.: Third trochanter. B, tibia. Abbreviations: A.s.t.: Articular surface for the talus; C.a.: Caudal apophysis; Ce.i.a.: Central intercondylar area; Cr.i.a.: Cranial intercondylar area; D.a.s.f.: Distal articular surface for the fibula; E.g.: Extensor groove; I.c.: Interosseous crest; L.a.s.: Lateral articular surface; L.c.: Lateral condyle; L.g.: Lateral groove; L.i.t.: Lateral intercondylar tubercle; M.a.s.: Medial articular surface; M.c.: Medial condyle; M.g.: Medial groove; M.i.t.: Medial intercondylar tubercle; M.m.: Medial malleolus; P.a.s.f.: Proximal articular surface for the fibula; P.n.: Popliteal notch; S.s.m.p.: Sliding surface for the m. popliteus; T.c.: Tibial crest; T.g.: Tuberosity groove; T.t.: Tibial tuberosity. C, fibula. Abbreviations: A.s.t.: Articular surface for the talus; Ca.l.: Caudolateral line; Ca.t.l.m.: Caudal tubercle of the lateral malleolus; Cr.l.: Craniolateral line; Cr.t.l.m.: Cranial tubercle of the lateral malleolus; D.a.s.t.: Distal articular surface for the tibia; D.g.m.: Distal groove of the malleolus; H.: Head; I.c.: Interosseous crest; L.g.: Lateral groove; P.a.s.t.: Proximal articular surface for the tibia.

Figure S2. Shape deformations associated with the first two axes of the PCA for each bone. Blue: minimal values. Orange: maximal values. Orientation from left to right: caudal, lateral, cranial, medial, proximal and distal views. A, complete femur; B, proximal partial femur; C, distal partial femur; D, tibia; E, fibula.

Figure S3. Shape deformations associated with minimum and maximum values of the centroid size (CS), body mass (BM) and gracility index (GI-MT3) for significant regressions with shape. Blue: minimal values. Orange:

maximal values. Orientation from left to right: caudal, lateral, cranial, medial, proximal and distal views. A-C, complete femur; D-F, proximal partial femur; G, distal partial femur; H-I, tibia; J, fibula.

Figure S4. Significant PGLS regression plots for distal partial femur (A) and fibula (B) performed on shape data and log-transformed centroid size (CS) or log-transformed cubic root of mean body mass (BM). Point colour code follows Figure 1. Point size is proportional to mean log CS of each species. On the right, shapes associated with minimum and maximum fitted values (top row) and colour maps of the location and intensity of the shape deformation (bottom row). Blue: minimal values. Orange: maximal values. For each bone, the shape associated with the minimum was coloured depending on its distance to the shape associated with the maximum (blue indicates a low deformation intensity and red indicates a high deformation intensity). Orientation from left to right in each case: caudal, lateral, cranial and medial views.

Figure S5. Boxplot of the distribution of GI-MC3 (from Mallet *et al.*, 2021) and GI-MT3 values (this work). Parametric tests indicate a high correlation between the two indices, and a high probability of similar mean and variance.

Table S1. Complete list of all the studied specimens.

Table S2. Complete list of data compiled from the literature for gracility index of third metatarsal and mean body mass.

Table S3. Summary of the differences in *P* and R^2 values between the PGLS computed under a Brownian Motion (BM) model (geomorph) and a Ridge Regression (RR) model (RRphylo). Only variables with significant results are presented here.